

## Article

# Peraluminous Rare Metal Granites in Iberia: Geochemical, Mineralogical, Geothermobarometric, and Petrogenetic Constraints

Francisco Javier López-Moro <sup>1,\*</sup>, Alejandro Díez-Montes <sup>1</sup> , Susana María Timón-Sánchez <sup>1</sup>,  
Teresa Llorens-González <sup>1</sup>  and Teresa Sánchez-García <sup>2</sup>

<sup>1</sup> IGME-CSIC, Oficina de Salamanca, Plaza de la Constitución 1, 37001 Salamanca, Spain; al.diez@igme.es (A.D.-M.); s.timon@igme.es (S.M.T.-S.); t.llorens@igme.es (T.L.-G.)

<sup>2</sup> IGME-CSIC, Ríos Rosas, 23, 28003 Madrid, Spain; t.sanchez@igme.es

\* Correspondence: fj.lopez@igme.es

**Abstract:** The intensive variables, geochemical, mineralogical, and petrogenetic constraints of the Iberian peraluminous rare metal granites (RMGs), many of them unknown, are presented. The mineral chemistry of ore and gangue minerals, whole rock analyses, geothermobarometry, melt water and phosphorus contents, mass balance, and Rayleigh modeling were performed to achieve these objectives. These procedures allow us to distinguish two main contrasting granitic types: Nb-Ta-rich and Nb-Ta-poor granites. The former have lower crystallization temperatures, higher water contents, and lower emplacement pressures than Nb-Ta-poor granites. Nb-Ta-rich granites also have higher fluoride contents, strong fractionation into geochemical twins, higher Na contents, and different evolutionary trends. At the deposit scale, the fractional crystallization of micas properly explains the variation in the Ta/Nb ratio in both Nb-Ta-poor and Nb-Ta-rich RMGs, although in higher-grade granites, the variation is not as clear due to the action of fluids. Fluid phase separation processes especially occurred in the Nb-Ta rich granites, thus transporting halogens and metals that increased the grades in the top and sometimes in the core of granites. Gas-driven filter pressing processes facilitated the migration of fluid and melt near solidus melt in Nb-Ta-rich granites. The geochemical signature of the Iberian rare metal granites mainly follows the trends of two-mica granites and P-rich cordierite granites, but also of granodiorites.

**Keywords:** rare metal granite; parental magma; exsolved fluid phase; albitization; Nb/Ta ratio; columbite group minerals; Iberian Massif



**Citation:** López-Moro, F.J.; Díez-Montes, A.; Timón-Sánchez, S.M.; Llorens-González, T.; Sánchez-García, T. Peraluminous Rare Metal Granites in Iberia: Geochemical, Mineralogical, Geothermobarometric, and Petrogenetic Constraints.

*Minerals* **2024**, *14*, 249. <https://doi.org/10.3390/min14030249>

Academic Editor: Xiaolei Wang

Received: 2 January 2024

Revised: 21 February 2024

Accepted: 25 February 2024

Published: 28 February 2024



**Copyright:** © 2024 by the authors. Licensee MDPI, Basel, Switzerland. This article is an open access article distributed under the terms and conditions of the Creative Commons Attribution (CC BY) license (<https://creativecommons.org/licenses/by/4.0/>).

## 1. Introduction

Recently, the European Union has funded research projects to determine the availability of critical metals (REE, Li, Nb, Ta, W, among others) in the European Union in the face of the challenge of ecological transition and the extensive use of electronic devices in our daily lives. ProMine, ORAMA, GeoERA, SCRREN, FutuRaM, and GSEU are good examples of such projects (see European Geological Data Infrastructure <https://www.europe-geology.eu/> accessed on 20 December 2023). Since the recycling processes of these metals do not cover more than a minimal part of the needs of the current industry, it is necessary to find or re-exploit mineral deposits that could contain these critical metals. Rare metal granites (RMGs) are good candidates. Although in many cases, these granites do not have high grades of these metals, they do have high tonnages, and in addition, they usually show alteration/weathering processes (kaolinization) that make their extraction and treatment in processing plants inexpensive, since they do not need to be crushed or even milled. Another advantage of the kaolinization process is that it can increase the concentration of the ore up to twofold by the mass losses of the silicate fraction [1].

In Iberia, rare metal granites were discovered in the last century and were the subject of studies in the 1970s and 1980s by mining companies and research centers, in most cases

paid by these companies, thereby mainly benefiting Sn and W and exceptionally Ta. These studies resulted in mostly internal reports that were difficult for the public to access, and, in exceptional cases, this information was used for the realization of doctoral theses and for publication in local research articles. A dramatic drop in the price of these metals in the mid-1980s led to the closure of all mines associated with these granites in Iberia. After 30–40 years, the high market prices of elements such as Ta, Nb, Sn, W, Be, REE have encouraged mining companies to look for new deposits or to re-evaluate the viability of the rare metal granites mined in the 1970s–1980s in Iberia, as in the case of the rare metal granites of Penouta (Strategic Minerals Europe), El Trasmorquión (Grabat Energy), Fuentes de Oñoro (SIEMCALSA, Berkeley), Golpejas (Solid Mines, Salamanca Ingenieros), Argemela (PANNN Consultores de Geociências Lda), and the alkaline orthogneisses of Galíñeiro (Umbono Capital), thereby generating more information [2–4]. In addition, European countries and the European Union have recently shown further interest in this type of deposit, thus funding research projects that have produced a great deal of information, both published [5,6] and unpublished.

RMGs, together with LCT rare metal pegmatites, represent very evolved acid melts that are strongly enriched in metal (Sn, Nb, Ta, W, Be, Li, U, and Hf), LILE (Rb and Cs) and fluxing elements (e.g., H<sub>2</sub>O, F, B, and P), as well as have strong depletions in Ca, Sr, Ba, REE, Ti, Fe, and Mg (e.g., Linnen and Cuney, 2005; London, 2008). However, there are clear differences between RMGs and LCT pegmatites, including the following: (i) grain size, which is extremely coarse in pegmatites and fine to medium in RMGs; (ii) zoning, which is very noticeable in LCT pegmatites from the margins inward—an aspect that does not seem to be so well constrained in RMGs; (iii) the mode of occurrence, as pegmatites always occur in sills or lens-like bodies, whereas RMGs can occur in stock-like bodies, but also in sills or lens-like bodies; (iv) the proportion of water and other fluxing elements, which is thought to be very high in pegmatites, actually represents water-saturated melts (see [7]), and is thought to be lower in RMGs; (v) metal grades, which are usually higher in pegmatites than in RMGs; (vi) differentiation processes, such as liquidus undercooling, nonequilibrium crystallization, or zone refining processes, which are very common in pegmatites [8,9] and are thought to be less common or absent in RMGs.

The origin of RMGs remains uncertain. The magma from which they are derived is not known with certainty, often because they occur in isolated stocks or tabular bodies, which means that their source area is not known either. Similarly, the process that leads to critical metal enrichments is poorly understood. It seems clear that there is a magmatic process of extreme differentiation that is strongly conditioned by the presence of fluxing elements (H<sub>2</sub>O, F, B, P or Li), which lower the granitic solidus and the viscosity, thereby favoring protracted crystal melt fractionation [10]. This extreme crystallization can enrich the melt in these critical metals, but it is not known in what proportion. On the other hand, in these granites, there is evidence of the saturation and exsolution of a fluid phase that could increase the concentrations of metallic elements. This could occur for elements with an affinity for the fluid phase, such as W, Sn, and Be, but it is not clear that the same happens with other metals, e.g., Nb and Ta, which have affinity for the melt [11,12]. This problem has led to the proposal of the existence of liquid immiscibility processes involving a brine/melt phase [13,14], but the existence of immiscibility processes in this type of melt does not have the support of the entire scientific community. Similarly, the upward injection of rare element-rich phases [15] or interstitial residual melt removed from deeper parts of the pluton [16] have also been proposed to explain the enrichment.

This work gathers all the available structural, geochemical, and chemical–mineralogical data generated by mining companies and research centers in the last 50 years, as well as chemical–mineralogical data to characterize the Iberian rare metal granites from a geochemical, mineralogical, and geothermometric point of view in order to distinguish the different rare metal granites in Iberia and to decipher the main factors that most control their peculiar geochemistry and mineralization itself.

## 2. Geological Setting

The Iberian RMGs are located in the Variscan Belt, which is the basement that formed along the Devonian, Carboniferous, and Early Permian [17]. From a tectonic point of view, the Variscan Belt is the result of the Devonian and Carboniferous collision between Gondwana, as well as some peri-Gondwana terranes and the Avalonian margin of Laurentia [18]. The early imprint of this collision was recorded by the development of active margins and arcs and the subsequent accretion of arc units onto continental blocks, thereby triggering HP/HT eclogite units and the accretion of ophiolites formed in suprasubduction environments [19]. Nappe stacking also was developed, with thrusting propagating to the outer zones, while inner parts underwent partial melting in the lower crust and extensional detachment, and thermal gneiss domes were formed (e.g., [20,21]). Late tectonic evolution developed synconvergent extension in the inner domains, crustal-scale transcurrent shear zones, and the intrusion of synkinematic magmas [22–24].

The NW Iberian Massif represents the innermost region of the Variscan Iberian Massif [17] and is characterized by high-T metamorphism and a large volume of Variscan granitic intrusions. There are several classifications that have attempted to establish a chronology of this important volume of granitoids. The classification of granitoids has been carried out in relation to the emplacement level [25–27], in relation to deformation [28], and in relation to the Variscan deformation, emplacement level, and the petrological–mineralogical characteristics [29]. More recently, [30,31] indicate that the Variscan granitoids can be mainly classified into five types. Four types are mostly peraluminous with S-type granite affinities. The last type granites have affinities to I-type granites [30,32].

In the Iberian Massif, the record of continental collision began ca. 365 Ma [33–35]. Carboniferous synorogenic magmatism began ca. 350–340 Ma in the hinterland of the orogen [36] and ended with a later to postorogenic magmatism at ca. 305–290 Ma [37–39]. Within the D3 synorogenic magmatism, the so-called early granodiorites of the Iberian Variscan belt represent a per- and metaluminous, biotite-rich synkinematic magmatism, often with tonalitic facies and K-Mg-rich magmatic rocks: the so-called vaugnerites. This indicates an important magmatic activity in the Visean period, which dates to ca. 347–335 Ma [39–43]. Another group of D3 synkinematic granitoids is represented by peraluminous two-mica granites, leucogranites, and adamellites. Their ages range from 322 Ma to 305 Ma, with a maximum between 310 and 305 Ma [42,44]. The development of extensional gneissic domes and migmatization with HT/LP metamorphism developed between 325 and 310 Ma [44,45]. This synkinematic magmatism is affected by ductile shear zones. Ages obtained from large-scale ductile shear zones in the western Iberia provide coeval ages that cluster around 310–305 Ma [46]. Later postorogenic magmatism peaked at ca. 305–285 Ma, with granitoid magmas emplaced in both the inner and outer zones of the orogen [47–50]. The late orogenic magmatism is represented by circumscribed massifs of porphyritic cordierite-bearing peraluminous granites that show an N-S orientation of potassium feldspar phenocrysts. These granitic massifs cut the ductile shear zones and have an age range of 305–295 Ma [49]. Finally, the postorogenic magmatism is metaluminous to slightly peraluminous and features I-type granites, as well as monzogranites ± granodiorites ± tonalites [32]. The age of this magmatism shows an age range of 295–290 Ma [50]. The scarce Variscan mafic magmatism is mainly concentrated in the range of 305–294 Ma, with a final manifestation represented by minor shoshonitic dykes [51].

There are few dated Iberian rare metal granites. The oldest geochronological data corresponds to the Argemela granite in Portugal, which yields an age of  $326 \text{ Ma} \pm 3 \text{ Ma}$  (U-Pb LA-ICP-MS CGM, [52]), i.e., in the D2 age tectonic phase [34,39]. It is followed by the Belvis de Monroy granite ( $314 \pm 3 \text{ Ma}$ , U-Th-Pb ID-TIMS in monazite, [53]) corresponding to the D3 contractional deformation in the CIZ [34,39]. Finally, the younger RMG age recorded in Iberia is the Logrosán granite, which has an age of  $307.9 \pm 0.86 \text{ Ma}$  (U-Pb ID-TIMS in zircon and monazite, [54]), which is coincident with the strike-slip shearing event in Iberia [46].

In the European Variscan Belt, RMGs extend from Iberia to the Bohemian Massif (Figure 1A). They outcrop in the Armorican Massif of France (e.g., Tréguennec; see [55]), the French Massif Central (e.g., Blond Massif, Montebbras, and Beauvoir and Chavance; see [55–58]), the Iberian Massif (Penouta and Argemela; see [2,3,5,59]), the Bohemian Massif (Podlesi and Cinovec/Zinnwald; see [60,61]), and Cornwall (e.g., the St. Austell granites and the Tregonning–Godolphin granite; see [62,63]). The European Variscan RMGs show geochemical differences depending on the area: French and Portuguese granites are richer in P, Al, Li, Sn, and Rb and have higher Ta/Nb ratios than those of the Bohemian and Cornwall massifs [64]. Granites from the Cornwall and Bohemian massifs have a geochemical affinity of A-type granites, and they are peraluminous, although they are less peraluminous than typical RMGs from the Massif Central or Iberian Massif. The reasons for these geochemical differences are poorly understood, but differences in source or partial melting temperature may be involved.

### 3. Occurrences of Rare Metal Granites in the Central Iberian Zone and Data Sources

In this paper, we will focus on granites in which rare metal ore is disseminated either in leucogranites or apical cupolas crystallizing from residual, granitophile element enriched magma that may also be metasomatized by Na-rich fluids (i.e., apogranites) that are located in the Central Iberian Zone and Galicia-Trás-os-Montes Zone, i.e., Group B1 as defined by [65]. The geological and mineralogical characteristics of economic and subeconomic occurrences of B1 granite are summarized in Table 1. Whole rock data used in this work were obtained from external sources (Table 1), and mineral analyses were obtained from external sources, except for minerals from the Golpejas granite analyzed in this work (Table 1).

We have distinguished two major groups of these granites, because they have different geochemical and geothermometric characteristics, as will be seen below: Nb-Ta-poor granites and Nb-Ta-rich granites. The group of Nb-Ta-rich rare metal granites includes the Penouta (Sn-Ta-Nb  $\pm$  Be), Golpejas (Sn-Ta-Nb  $\pm$  Li), Argemela (Li-Sn-Ta-Nb), Villardeciervos (Sn-Nb-Ta), Fuentes de Oñoro (Li-Sn-Ta-Nb), and Tres Arroyos (W-Li-Nb-Ta) granites (Figure 1A). The group of Nb-Ta-poor granites includes the granites of El Trasquilón (Sn-Li  $\pm$  Nb  $\pm$  Ta), Fontao (W  $\pm$  Sn  $\pm$  Nb), Logrosán (Sn  $\pm$  Nb), Laza (Sn  $\pm$  Ta), Ponte Segade (W  $\pm$  Nb  $\pm$  Ta), Beariz (Sn  $\pm$  Nb  $\pm$  Ta), Acebo (Li-W  $\pm$  Nb), Torrecilla de los Ángeles (Sn-W  $\pm$  Li), Belvis de Monroy (Be  $\pm$  Li), Pedroso de Acim (W-Sn-Li  $\pm$  Nb  $\pm$  Ta), and Jálama (Li  $\pm$  Nb) (Figure 1B). In these granites, mainly Sn or W has been mined, while the beneficiation of Nb-Ta has been scarce and limited in the 1980s to the Golpejas and Penouta granites and currently to the Penouta granite. There is no evidence of Li mining in these granites. The most extensively mined rare metal granites, due to their high grades and/or reserves, are the albite granites of Penouta and Golpejas, as well as the granites of Fontao and El Trasquilón. A brief description of the most important Iberian RMGs is shown below.

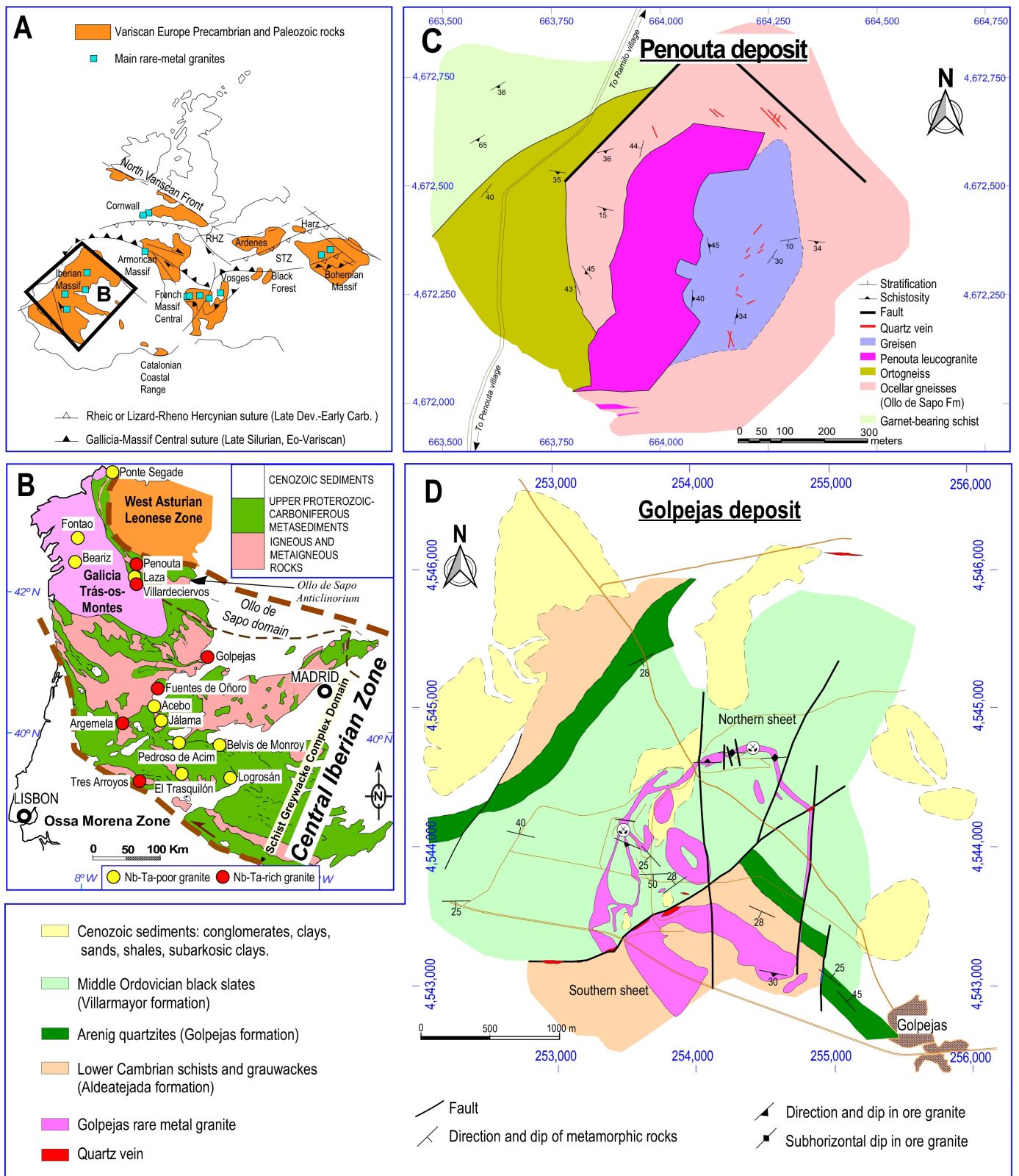


**Figure 1.** (A) Schematic map of the Variscan orogen in Europe (based on [66]), including main RMGs. (B) Location of Iberian rare metal granites in the Central Iberian Zone and Galicia-Trás-os-Montes Zone (Spain and Portugal). (C) Geological map of the Penouta deposit (modified from [2]). (D) Geological map of the Golpejas deposit (modified from [67]).

**Table 1.** Iberian RMGs' outstanding characteristics and source of data.

Occurrence	Granite Type	Primary Geology Features	Mineralization	Maximum Ore Content (ppm)	Reserves (Mt)	Whole Rock Source	Mineral Chemistry Source
Penouta	AG/LP/NbTa-rich	Isolated, undeformed, lens-like body	Sn-Ta-Nb ± Be	Sn: 3800; Ta: 226	>10	[2,68]	[3,4,69]
Golpejas	AG/HP/NbTa-rich	Isolated, deformed, sheet shape, Q-Aby dykes	Sn-Ta-Nb ± Li	Sn: 2097; Ta: 215	5–10	[69,70]	This work
Argemela	AG/HP/NbTa-rich	Isolated, deformed, piston-like body	Li-Sn-Ta-Nb	Sn: 1960; Ta: 161	Unknown	[5,15,59]	[5,59]
Villardecervos	AG/NbTa-rich	Apophysis, related to two mica granite	Sn-Nb-Ta	Sn: 439; Ta: 273	1–5	[71,72]	-
Fuentes de Oñoro	AG/MP/NbTa-rich	Apophysis, related to biotite granite	Li-Sn-Ta-Nb	Sn: 500 *; Ta: 50 *	<1	[73]	-
Tres Arroyos	LG/MP/NbTa-rich	Leucocratic dyke, undeformed	W-Li-Nb-Ta	Sn: 781; Ta: 124	<1	[74,75]	[74]
El Trasmullón	AG/HP/NbTa-poor	Cupola, kaolinization, Q-Aby dykes	Sn-Li ± Nb ± Ta	Sn: 5830; Ta: 78	1–5	[69,74,76]	[74]
Fontao	2M/MP/NbTa-poor	Isolated, cupola, undeformed	W ± Sn ± Nb	W: 266; Ta: 13	1–5	[69]	-
Logrosán	LG/MP/NbTa-poor	Isolated, undeformed, stock,	Sn ± Nb	Sn: 1000; Ta: 5.7	<1	[54,77]	[54,77]
Laza	LG/NbTa-poor	Sheet shape, muscovite-rich granite	Sn ± Ta	Sn: 2300; Ta: 10	5–10	[78]	-
Ponte Segade	AG/MP/NbTa-poor	Apophysis, related to two mica granite	W ± Nb ± Ta	Sn: 110; Ta: 7	<1	[79]	[79]
Beariz	2M/MP/NbTa-poor	Isolated, muscovite-rich in border facies	Sn ± Nb ± Ta	Sn: 105; Ta: 45	<1	[80]	[80]
Acebo	LC/NbTa-poor	Cupola, albitization, kaolinization	Li-W ± Nb	Sn: 60; Ta: 40	1–5	[81]	-
Torreçilla	2M/NbTa-poor	Cupola, albitization, kaolinization	Sn-W ± Li	Sn: 7200; Ta: -	1–5	[81]	-
Belvis de Monroy	LG/MP/NbTa-poor	Isolated, reversely zoned pluton	Be ± Li	Sn: 50; Ta: 5	Unknown	[82]	-
Pedroso de Acim	2M/MP/NbTa-poor	Isolated, apophysis, Bt-bearing	W-Sn-Li ± Nb ± Ta	Sn: 602; Ta: 29	<1	[74,81,83]	-
Jálama	2M/MP/NbTa-poor	Border facies of a big pluton	Li ± Nb	Sn: 44; Ta: 7	Unknown	[84]	-

AG: albite granite; LG: leucogranite; 2M: two-mica granite; LP: low-phosphorus granite; HP: high-phosphorus granite; MP: medium-phosphorus granite; LP: low-phosphorus granite; reserves from [65]; \*: determined by portable XRF analyzer in this work; -: Not reported or referenced.

### 3.1. The Penouta Sn-Ta-Nb ± Be Albite Granite

The Penouta granite outcrops in an area of about 0.2 km<sup>2</sup>, and in its present state (strongly influenced by the old mining activities), it is elongated in a north–south direction (Figure 1B). This granite is a lenticular body emplaced in the hinge of a D3 Variscan antiform [45,85] following the planar anisotropies of the wall rocks, which are mainly the orthogneiss of the Ollo de Sapo Fm and the paragneiss of the Viana do Bolo series [2]. Two main granitic facies can be distinguished: A fine-grained, muscovite-rich granite at the base of the body with Sn-Nb-Ta ore and significant Be contents and a fine-grained, albite-rich granite at the apical zone of the body where the ore grade is higher. The mineralization mainly consists of magmatic disseminated cassiterite and columbite-group minerals with up to 226 ppm Ta, 89 ppm Nb, and up to 0.38% Sn (Table 2). Flat-lying sheets of aplopegmatite can be found in the Penouta granite, especially in the apical zone. These are nearly horizontal tabular bodies that are centimeters to meters thick and composed of different proportions of the main constituents (e.g., quartz–mica layers, albite layers, and quartz layers) that are rhythmically sandwiched. This granite developed, especially in the eastern zone, a Sn-enriched greisen (without Nb-Ta ore) in overlying metamorphic rocks. Mineralogically, the granite consists of quartz, albite, potassium feldspar, and white mica as major minerals, with garnet, beryl, zircon, apatite, monazite, fluorite, cassiterite, and Nb-Ta oxides as accessory minerals [2–4]. There are mineralogical differences between the two facies mainly in terms of modal proportions, with a higher proportion of muscovite, garnet, and quartz in the deeper facies, while the apical facies is richer in albite. In addition, fluorite and wodginitite have been identified only in the apical facies. Kaolinite is a secondary mineral mainly developed in the weathered leucogranite, and its occurrence favored the mining of the deposit in the 1980s.

### 3.2. The Golpejas Sn-Ta-Nb ± Li Albite Granite

The Golpejas granite consists of several sheets of mineralized albitic granite with a semicircular shape [86] (Figure 1C). These sheets range from 7 to 35 m thick and dip outward from 30° to 72°. The grain size of the granite in these sheets varies from fine at the margins to medium grain in the central part. The presence of a subhorizontal solid state deformation fabric is prominent, especially in the deepest areas. It is a zoned body where the fresh margin is richer in albite than the quartz-rich core [86]. The mineralization consists mainly of magmatic disseminated cassiterite and columbite group minerals in the leucogranite. To the north, where the highest tin and Nb-Ta grades are found, the granite is strongly kaolinized, thereby resulting in high grades in most cases by mass loss [1]. Ore content can reach about 230 ppm for Nb and 215 ppm for Ta and up to 0.2% Sn (Table 2). The granite consists of quartz, albite, potassium feldspar, and white mica as major minerals and zircon, cassiterite, Nb-Ta oxides, apatite, and aluminum phosphates as accessory minerals. In the contact zone of this body with pelites, a greisen was developed with a thickness ranging from a few millimeters to 20 cm. Intragranitic quartz veins also occur containing Li minerals (amblygonite group minerals), Cu, Sn, Zn, Ag and Bi sulfides, iron oxides, and carbonates [86]. These quartz veins are often subhorizontal and subparallel to the granite foliation and occur mainly in the apical zone.

**Table 2.** Whole rock data and thermometric results of representative Iberian RMGs.

Granite	Golpejas			Penouta			Argemela			El Trasquilón			Logrosán		
	Max	Av	Std	Max	Av	Std	Max	Av	Std	Max	Av	Std	Max	Av	Std
SiO <sub>2</sub> (wt.%)	74	69.66	3.39	77.20	74.26	1.45	74.41	69.69	5.26	76.60	71.22	2.15	74.03	70.52	6.22
TiO <sub>2</sub>	0.05	0.05	0.00	0.01	0.00	0.00	0.07	0.05	0.27	0.09	0.05	0.01	0.33	0.19	0.06
Al <sub>2</sub> O <sub>3</sub>	24.2	16.30	2.19	18.20	15.71	0.66	21.02	17.31	3.57	21.10	17.00	1.63	31.61	16.49	4.25
FeOt	0.57	0.31	0.11	1.02	0.49	0.22	0.57	0.28	0.12	1.91	0.89	0.25	2.18	1.30	0.38

Table 2. Cont.

Granite	Golpejas			Penouta			Argemela			El Trasquilón			Logrosán		
	Value	Max	Av	Std	Max	Av	Std	Max	Av	Std	Max	Av	Std	Max	Av
MnO	0.16	0.07	0.06	0.20	0.05	0.05	0.06	0.03	0.02	0.49	0.06	0.07	0.04	0.02	0.01
MgO	0.16	0.11	0.04	0.09	0.03	0.01	0.04	0.03	0.17	0.31	0.20	0.06	0.75	0.31	0.14
CaO	3.39	1.63	1.35	0.19	0.14	0.02	1.71	0.23	0.36	1.52	0.59	0.37	0.69	0.42	0.15
Na <sub>2</sub> O	6.94	5.07	0.82	7.74	6.10	0.90	9.30	5.46	2.02	4.59	3.23	0.97	4.28	3.10	0.66
K <sub>2</sub> O	4.16	3.14	0.61	4.07	3.30	0.36	5.16	2.56	1.12	5.37	3.37	0.65	8.50	4.87	1.03
P <sub>2</sub> O <sub>5</sub>	2.63	1.32	0.98	0.07	0.05	0.01	2.69	1.71	0.85	2.59	1.08	0.43	0.78	0.51	0.15
LOI	2.14	1.55	0.44	-	-	-	4.49	1.65	0.74	3.20	2.03	0.44	5.86	1.96	1.55
Total	100.4	100.3	0.15	102	100.2	1.01	100.3	98.9	0.68	101.1	99.75	0.86	99.99	98.6	0.87
A/CNK	1.55	1.13	0.19	1.83	1.14	0.11	2.01	1.56	1.04	2.26	1.84	1.01	2.73	1.49	0.37
A/NK	1.58	1.39	0.12	1.87	1.16	0.11	2.16	1.61	1.04	2.46	2.06	1.12	2.76	1.59	0.35
F (ppm)	15,749	3249	3630	-	-	-	12,500	4875	3287	5800	2457	1582	5495	1002	1534
Li	1084	86	98	129	129	-	5532	1607	1634	4555	318	413	780	132	209
Rb	2184	1030	282	1105	892	114	2448	1224	613	985	792	87	918	363	156
Cs	97	27.82	20.39	56.00	34.98	7.02	350	89.97	99.86	81.00	81.00	-	275	70.32	66.55
Ba	145	45.10	42.95	141.50	17.43	26.18	53	9.61	11.16	19.00	9.14	6.07	290	200	51.72
Sr	875	86.41	204.88	62.60	17.38	14.00	677	42.83	113.3	90.00	37.09	24.70	77.00	44.50	13.47
Pb	18	6.03	4.51	-	-	-	34.50	9.68	10.12	8.00	6.43	1.40	40.00	19.81	12.42
Cr	67	7.21	18.06	10.00	4.91	5.05	5.20	1.39	1.67	-	-	-	-	-	-
Ni	43	12.58	11.80	-	-	-	8.31	0.80	1.82	16.00	6.29	5.99	20.00	16.25	8.06
V	77	5.84	19.65	-	-	-	0.00	0.00	0.00	-	-	-	21.00	9.59	4.37
Cu	75.5	17.27	22.02	-	-	-	36.64	8.71	9.32	-	-	-	50.00	12.50	11.83
Zn	139	64.22	23.19	0.72	0.28	0.13	134.0	45.53	39.79	116.0	89.57	20.74	100	44.24	30.88
As	24.3	6.84	6.36	-	-	-	103.9	13.63	29.10	266.0	95.00	84.22	1470	170.50	354.6
Sc	-	-	-	-	-	-	0.22	0.01	0.04	-	-	-	6.00	2.44	1.71
Sn	2097	296	359.4	3800	521	449.4	1960	686	453.2	5830	257	653	1000	114	242.0
Nb	230	115	32.1	89	68	9.1	91	50	21.1	97	35	12.5	21.3	13	3.9
Ta	215	105	32.1	226	73	38.5	161	62	36.8	78.5	13	11.9	5.7	3	1.1
W	17.4	5.96	5.37	5.00	2.51	0.72	58.80	7.39	9.63	-	-	-	376	95.68	119.4
Zr	39	29.67	5.09	31.00	20.21	4.52	28.60	13.64	4.10	139	59.67	22.25	118	74.00	19.78
Hf	7.83	5.41	1.21	8.50	6.87	0.87	5.36	2.73	1.05	6.21	2.91	0.78	3.10	2.29	0.56
Th	20	2.13	4.83	3.77	2.67	0.35	1.45	0.40	0.30	2.10	0.50	0.74	19.90	8.08	4.15
U	37.9	8.65	10.15	15.80	10.62	2.66	39.00	8.36	5.87	50.00	34.00	13.01	15.50	9.29	2.50
Ga	329	37.31	26.37	44.70	35.50	2.84	68.00	33.51	11.30	53.00	41.14	6.41	91.00	27.81	17.44
Be	103	44.76	33.41	125	125	-	385	95.44	84.30	-	-	-	23.00	11.00	6.95
Ge	8.46	4.05	1.58	-	-	-	5.54	2.13	2.31	-	-	-	3.80	1.98	1.14
Y	9.07	0.90	2.28	9.80	3.34	1.43	1.35	0.18	0.23	20.50	8.52	3.06	13.10	6.66	2.34
La	0.41	0.16	0.13	1.80	0.74	0.31	0.61	0.17	0.16	9.98	3.95	1.58	21.80	13.13	4.19
Ce	0.82	0.30	0.26	4.70	1.94	0.83	3.30	0.28	0.51	22.50	8.82	3.52	50.20	29.48	9.66
Pr	0.1	0.04	0.03	-	-	-	0.21	0.02	0.03	2.86	1.10	0.44	6.42	3.04	1.92

Table 2. Cont.

Granite	Golpejas			Penouta			Argemela			El Trasquilón			Logrosán		
	Value	Max	Av	Std	Max	Av	Std	Max	Av	Std	Max	Av	Std	Max	Av
Nd	0.6	0.23	0.19	3.10	1.09	0.53	1.32	0.08	0.20	11.77	4.56	1.81	25.80	13.39	4.95
Sm	0.77	0.09	0.21	4.23	1.86	0.77	0.45	0.03	0.07	4.52	1.69	0.68	5.18	3.01	1.01
Eu	0.3	0.05	0.10	0.11	0.02	0.03	0.31	0.01	0.05	0.15	0.03	0.03	0.58	0.32	0.11
Gd	2.19	0.21	0.60	8.01	3.89	1.48	0.53	0.03	0.08	5.20	2.03	0.81	3.64	2.30	0.64
Tb	0.36	0.09	0.10	1.46	0.76	0.25	0.06	0.00	0.01	1.05	0.41	0.16	0.54	0.34	0.09
Dy	1.76	0.24	0.52	4.19	1.57	0.64	0.27	0.02	0.05	4.99	2.00	0.77	2.22	1.57	0.39
Ho	0.31	0.05	0.10	0.12	0.04	0.02	0.04	0.00	0.01	0.63	0.25	0.10	0.34	0.23	0.06
Er	0.76	0.09	0.20	0.17	0.02	0.03	0.08	0.02	0.03	1.31	0.53	0.20	0.86	0.55	0.15
Tm	0.09	0.02	0.03	0.01	-	-	0.01	0.00	0.00	0.14	0.06	0.02	0.12	0.08	0.02
Yb	0.45	0.11	0.15	0.18	0.03	0.04	3.00	0.09	0.46	0.85	0.35	0.13	0.71	0.47	0.12
Lu	0.06	0.01	0.02	0.02	0.00	0.01	0.01	0.00	0.00	0.10	0.05	0.02	0.11	0.07	0.02
∑REE	7.79	1.40	1.96	26.36	11.98	4.56	5.16	0.76	1.00	65.93	25.82	10.14	117.0	67.96	22.28
T Zrn (°C)	690	657	19.10	687	636	16.98	657	621	21.56	818	739	28.28	778	745	20.51
T Mnz	527	417	61.59	680	597	31.87	543	354	174.3	777	676	36.70	806	760	31.06
T Ap	1010	556	310.1	708	513	70.27	1049	759	145.8	894	672	89.42	811	637	129.1

Source of data: Golpejas [69,70]; Penouta [2,68]; Argemela [5,15,59]; El Trasquilón [69,74,76]; Logrosán [54,77]; Max: highest value; Av: average; Std: standard deviation; -: not determined or below detection limit; T<sub>Zrn</sub>: saturation temperature of zircon according to the formulation of [87]; T<sub>Mnz</sub>: saturation temperature of monazite according to the formulation of [88]; T<sub>Ap</sub>: saturation temperature of apatite according to the formulation of [89].

## 4. Methods

### 4.1. Mineral Chemistry

In this work, we have determined only the chemical–mineralogical composition of the Nb-Ta oxides and silicates of the Golpejas granite (Table S1); the rest of the data used in this work come from external sources (see Table 1).

Quantitative chemical analyses of Ta and Nb oxide minerals were carried out on carbon-coated thin sections using a JEOL Superprobe JXA-8900 M with WDS at the Electron Microscopy Service of the Complutense University of Madrid. The analytical conditions consisted of an acceleration voltage of 15 kV, a beam current of 20 nA, a beam diameter of 1–5 μm, and counting times of 10 s. Standards used in analytical procedure include metals (W, Sn) zircon (Si, Zr), MnO<sub>2</sub> (Mn), LiNb (Nb), KaerTR (Na, Ca), hafnon (Hf), almandine (Fe), apatite (P, Cl, F), LiTa (Ta), UO<sub>2</sub> (U, Th), and IlmeTR (Ti).

A CAMEBAX SX-100 with WDS was also used to obtain quantitative chemical analyses of silicates at the Scientific and Technical Services of the University of Oviedo. The analytical conditions consisted of an acceleration voltage of 15 kV, a beam current of 15 nA, a beam diameter of 2 μm, and counting times of 5 s. Standards used in analytical procedure include metals (Ni, Sn, W), orthoclase (K), andradite (Ca), MnTi (Ti, Mn), magnetite (Fe), albite (Na), jadeite (Si), Al<sub>2</sub>O<sub>3</sub> (Al), MgO (Mg), apatite (P, F), chromite (Cr), vanadinite (Cl), covellite (Cu), Aspy\_mac (As), celestine (Sr), Nb\_mac (Nb), celsian (Ba), and Ta\_mac (Ta).

### 4.2. Geothermobarometry

Thermometric estimates were constrained by the saturation of zircon [87], monazite [88], and apatite [89]. Pressure conditions were estimated using the phengite barometer [90], and, when available, we reported microthermometric studies.

#### 4.3. Water Content

Magma water content was estimated from the empirical model based on the  $H_2O$  (vapor) =  $H_2O$  (melt) equilibrium of [91] for an  $X_{H_2O}$  in vapor of 1, pressure conditions were estimated from the microthermometry, and thermometric estimates were obtained from zircon saturation. Samples showing kaolinization and phengitization were excluded.

#### 4.4. Numerical Modeling

The liquid line of descent was performed using thermodynamic modeling with the Rhyolite-MELTS code [92], mass balance modeling was performed with the OPTIMASBA code [93], and Rayleigh modeling was performed with the FC-AFC-FCA code of [94]. The OPTIMASBA program uses multiple linear regression to perform mass balance calculations. For example, in a fractional crystallization process, it is necessary to consider a parent magma, minerals that fractionate, and an evolved magma that is to be obtained by subtracting from the composition of the parent magma different proportions of the minerals that fractionate. The validity of the obtained result is made by least squares fitting. The FC-AFC-FCA code performs different modeling with trace elements and isotopes. For instance, in fractional crystallization, the program uses a cumulated mineral mode, partition coefficients of trace elements that vary depending on the acidity of the melt, and different formulations of fractional crystallization, with the most commonly used being the Rayleigh formulation.

#### 4.5. P Content in the Melt

The P content in the melt was determined according to London's method [95]. For this purpose,  $D[P]_{Af}/melt$  was calculated according to the expression  $D[P]_{Af}/melt = 2.05474 \times \text{index ISA} - 1.74971$ , where  $ISA = (Al/(Ca \times 0.5 + Na + K + Rb + Li))$  in moles %. P in potassium feldspars and P in plagioclase were then averaged and averaged with both values. The resulting average value was divided by the previously obtained  $D[P]_{Af}/melt$  value to obtain the P value in the melt. This method permits comparison of the composition of P in the melt with the actual P content of the whole rock, and it permits us to check the following: (i) if the P remained immobile, i.e., when both contents are identical or similar and (ii) if the P in the melt is higher than the P in the whole rock, which is commonly accepted to reflect both the removal of P-enriched residual melts by filter pressing and the loss of P during the hydrothermal alteration of alkali feldspar (Figure 2C,D) (see [95,96]).

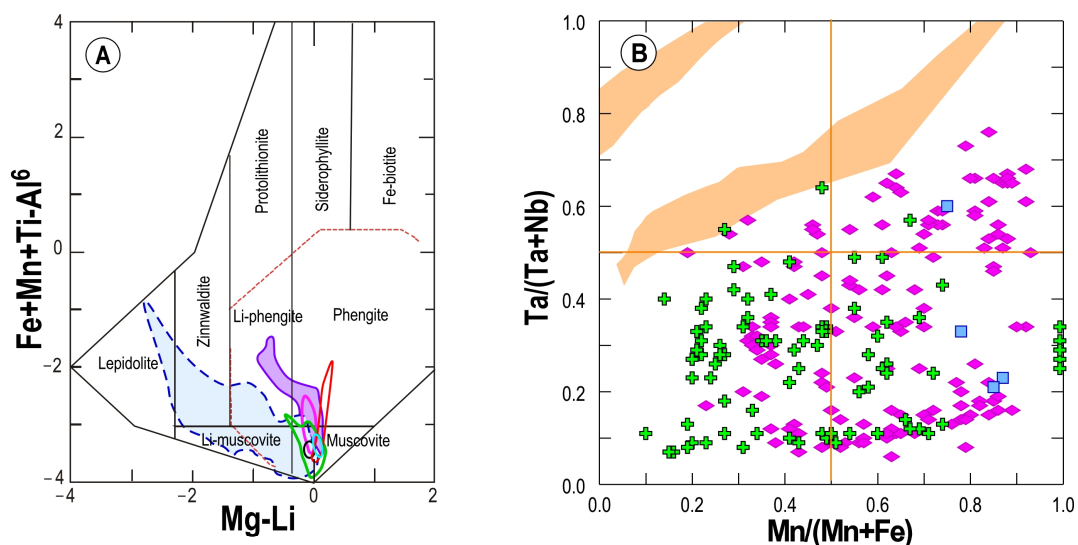
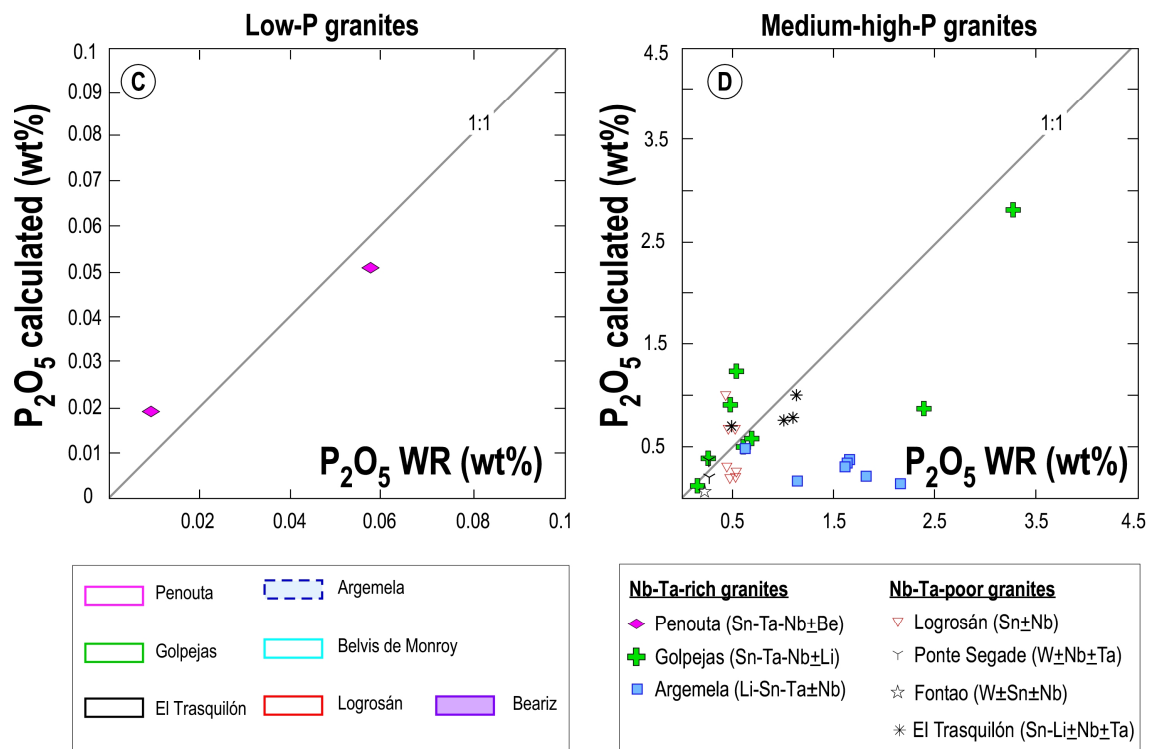


Figure 2. Cont.



**Figure 2.** Mineral chemistry constraints. (A) Classification of white micas for different Iberian rare metal granites according to the diagram of [97]. (B) Classification of Nb-Ta oxides in the CGM quadrilateral. Areas in orange represent compositional fields of cogenetic CGM and tapiolite according to [98]. (C,D)  $P_2O_5$  whole rock content vs.  $P_2O_5$  in melt from  $P_2O_5$  in alkali feldspar applied to low-P rare metal granites (C) and medium- and high-P rare metal granites (D).

#### 4.6. Portable XRF Analyses

Sn, Nb, and Ta of the Fuentes de Oñoro granite were determined using energy dispersive X-ray fluorescence (Bruker S1 Titan). Pieces of rock were ground into a powder with a particle diameter of less than 75 microns. The powder was packed into snap-closure polyethylene sample bags that were placed on a mobile test stand. An XRF exposure time of 180 s was used in the MINING Cu-Zn mode.

## 5. Results

### 5.1. Mineral Chemistry

#### 5.1.1. White Mica

The composition of the white micas of the Iberian rare metal granites is shown in Table S1. All data have been plotted in the diagram of [97], where most of the granites showed Li-poor micas. Indeed, muscovite was the most abundant, with some occurrence in the phengite field (Logrosán, Penouta and Beariz granites) and in the Li-phengite field (Beariz and Golpejas granites). The Argemela granite was quite different, thereby showing a very wide range of variation with muscovite, Li-muscovite, Li-phengite, zinnwaldite, and lepidolite (Figure 2A).

#### 5.1.2. Alkali Feldspars

The potassium feldspar of Iberian rare metal granites was generally K-rich (99.4–83.7 Or%, average 96.15 Or%), Na-poor (15.8–0.4 Ab%, average 3.71 Ab%), and Ca-poor (1.49–0 An%, average 0.08 An%) (see data Table S1). The  $P_2O_5$  contents in the K-feldspar ranged from 1.5% to values below the detection limit of the EMPA, with the Golpejas and Logrosán granites showing the highest contents, i.e., both Nb-Ta-rich and Nb-Ta-poor granites can have high P contents (see Table S1).

The plagioclase of the Iberian rare earth granites was albite (3.47–0.04%An, see Table S1). The  $P_2O_5$  contents ranged from 0.9% to values below the detection limit of the EMPA, with high values in both Nb-Ta-rich and Nb-Ta-poor granites (see Table S1). It is noteworthy that the  $P_2O_5$  contents in the plagioclase were lower than in the K-feldspar.

Moreover, in Nb-Ta-rich granites such as Argemela and Golpejas, the P in the melt estimated from alkali feldspar was relatively low compared to the P content in the whole rock (Figure 2D). Conversely, in some samples from Golpejas, the P in the melt may be higher than that in the whole rock (Figure 2D). Also note that the low-phosphorous granite from Penouta had P values in the melt that were very similar to those in the whole rock (Figure 2C). Finally, it should be noted that the range of variation between the P in the melt and the whole rock was significantly lower in the Nb-Ta-poor granites than in the Nb-Ta-rich granites (Figure 2D).

### 5.1.3. Columbite Group Minerals

The disseminated ores of the Nb-Ta oxides of the Iberian rare metal granites (Penouta, Argemela and Golpejas, i.e., Nb-Ta-rich granites) mostly corresponded to the columbite supergroup, namely the Columbite Group Minerals (CGM) (Figure 2B, Table S1). In the Penouta deposit, microlite, wodginite, and ferrotapiolite have also been reported [3,4]. In the CGM, columbite (i.e., oxides with  $Ta^* < 0.5$ , with  $Ta^* = Ta/(Ta + Nb)$ ) was more abundant than tantalite (i.e., oxides with  $Ta^* > 0.5$ ), with the former being particularly abundant in Golpejas, where it reached 95% of the total analyses. The Penouta deposit, on the other hand, was the one where tantalite was more abundant, reaching 33% of the total analyses. Manganese-rich CGM ( $Mn^* > 0.5$ , where  $Mn^*$  is equal to  $Mn/(Mn + Fe)$ ) were very abundant in Argemela (100%) and Penouta (73%), whereas iron-rich CGM ( $Mn^* < 0.5$ ) were predominant in Golpejas, where 66% of the available analyses corresponded to ferrous CGM.

## 5.2. Whole Rock Geochemistry

### 5.2.1. Major Element Compositions

Iberian rare metal granites were found to have silica contents ranging from 63 to 77 weight percent (Figure 3), with the lowest values typical of the border facies, which can be either albite-rich and/or mica-rich (see [5,59]).  $Al_2O_3$  was also quite variable, ranging from high concentrations (24 wt.%) in the Golpejas granite to 13 wt.% in quartz-rich samples from the Penouta albite granite (Figure 4). Most samples were peraluminous (average A/CNK = 1.33), although there were exceptions with values below one in P-Ca-rich samples from Golpejas (Figure 3A,F). The A/CNK index in these samples was clearly underestimated by the Ca control of apatite, and when the Ca excess was removed by the extraction of stoichiometric P, these samples showed a peraluminous signature, as shown in the graph of [99] (Figure 3B). The low Ti, Fe, Mg, and Mn contents of these granites, often below the detection limit, are typical of highly evolved magmas, with very limited femic minerals, restricted to ore minerals (CGM and cassiterite), garnet (in Penouta and Fontao), and Fe oxyhydroxides. The  $P_2O_5$  contents varied between low ( $<0.1 P_2O_5\%$ ) to high phosphorus granites ( $>0.9 P_2O_5\%$ ) according to [100] (Figure 3E). It is noteworthy that the phosphorus-rich samples from the Golpejas granite had higher CaO contents than other analogous P-rich rare metal granites as in the Argemela (Figure 4 and Table 2), probably because in Golpejas the predominant phosphate is apatite, while in Argemela the minerals of the amblygonite–montebrasite series dominate. Except for the P-Ca-rich samples from Golpejas, the rest of the samples can be classified as felsic peraluminous in the A-B plot of [101] (Figure 3F). The cationic Q-P diagram of [101] shows that most of the Nb-Ta-poor samples were granites and adamellites, whereas the Nb-Ta-rich granites were mostly plotted in the granodiorite field and with excursions to tonalite and other fields with a very negative P index (Figure 3C). Albite enrichment of Nb-Ta-rich granites could be the reason to explain the behavior of the Nb-Ta-rich granites. The agpaite index versus the Zr+Nb+Ce+Y diagram of [102] and the Rb-(Y+Nb) diagram of Pearce [103] were

used to determine whether the RMGs were alkaline or highly peraluminous (Figure 3F,G). Whalen’s plot shows a large scatter in the apatitic index. Most of the Nb-Ta-poor granites projected into the field of fractionated felsic granites, while the Nb-Ta-rich granites either projected into the field of A-type granites (Penouta) or, with a large dispersion, into all three fields (A-type, felsic granites -FG-, and unfractionated M-, I-, and S-type granites -OGT-). Since the Rb-(Y+Nb) diagram shows that all samples were within the synorogenic field, it can be excluded that they are A-type granites (see [104]). Therefore, the dispersion of the apatitic index suggests that it is sensitive to processes of enrichment in apatite and albite, which lower and raise this index, respectively (Figure 3G).

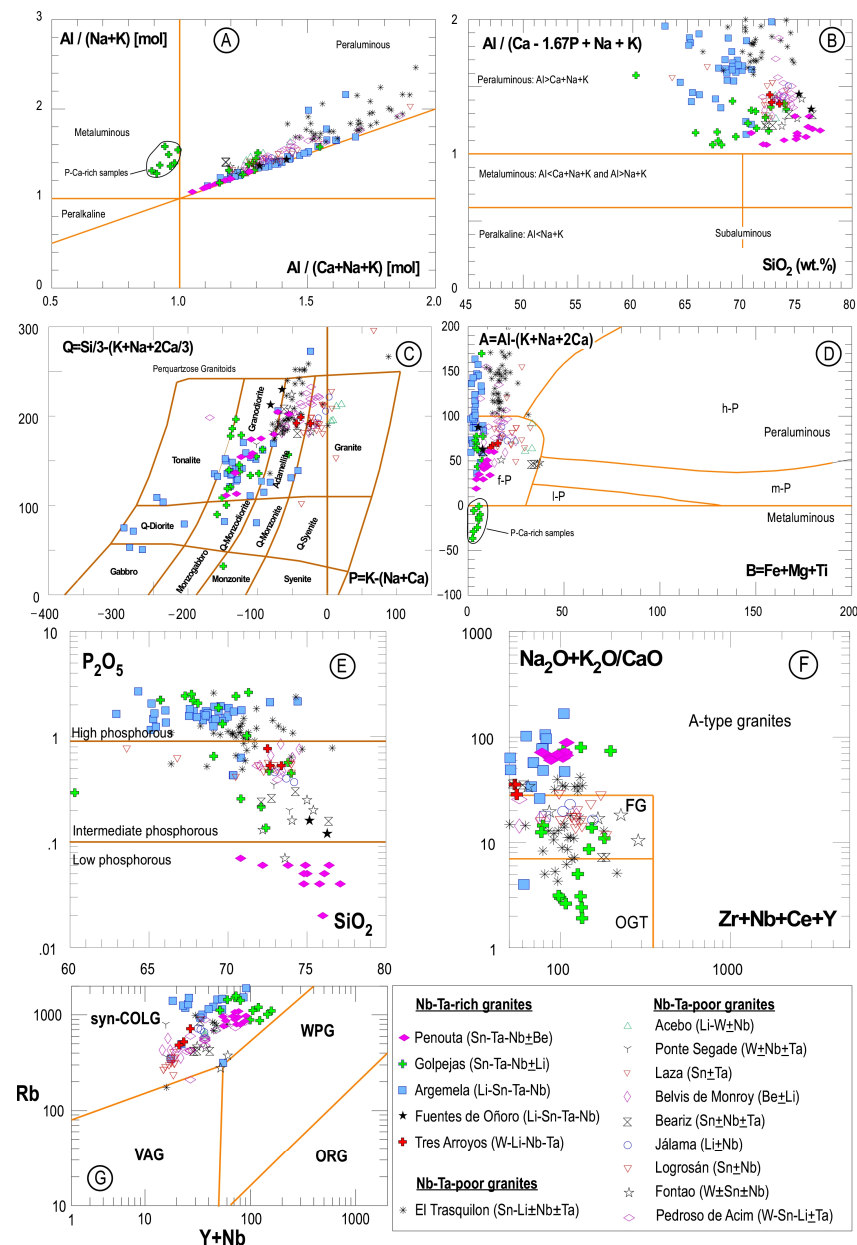
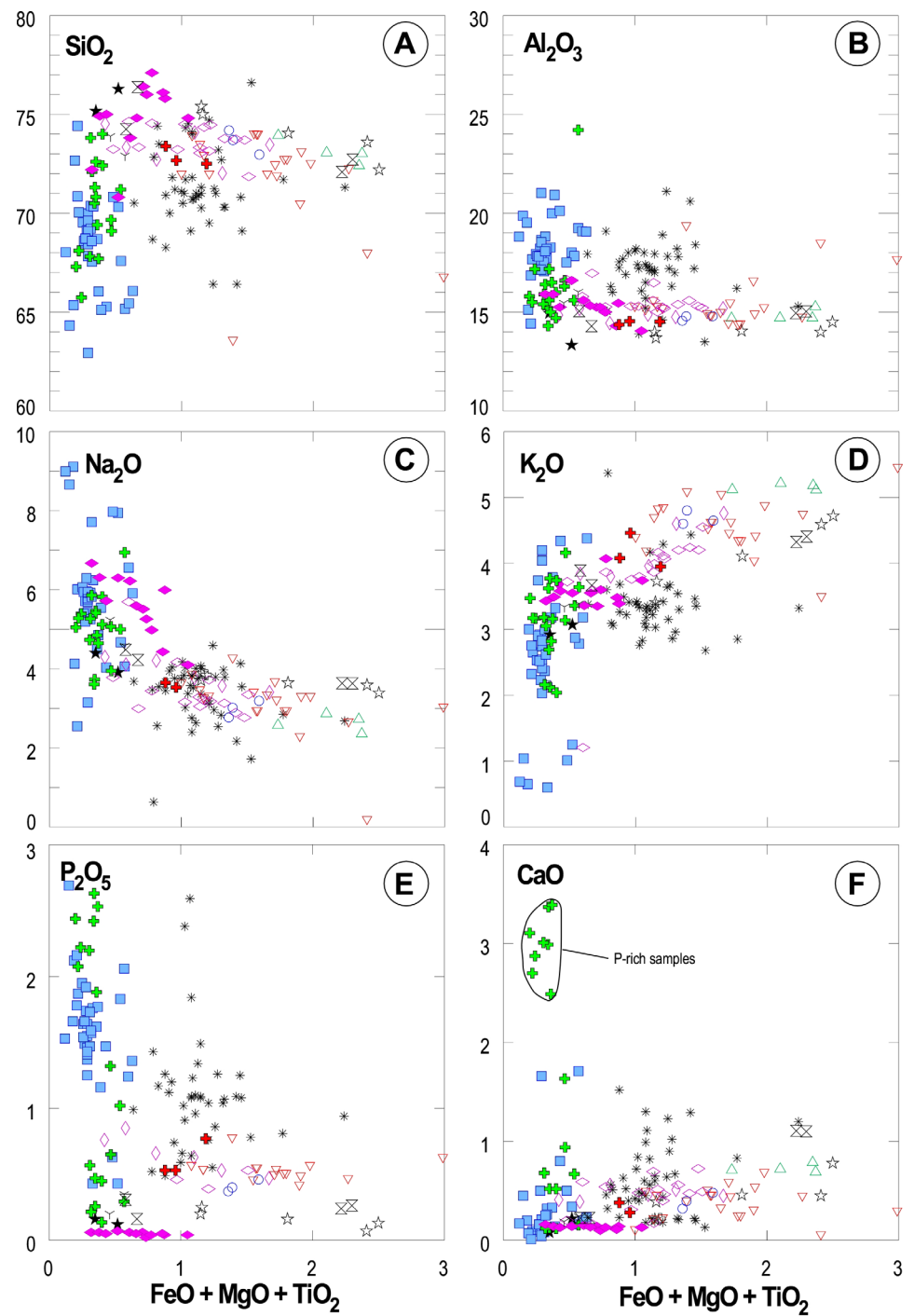


**Figure 3.** Classification diagrams. (A) Diagram of [105] applied to Iberian rare metal granites. (B) SiO<sub>2</sub>–aluminum saturation index plot of [99]. (C) Q–P cationic plot of [101]. (D) A–B multicationic plot of [101], modified by [106]. (E) P<sub>2</sub>O<sub>5</sub>–SiO<sub>2</sub> diagram including fields with different P contents. Fields after [100]. (F) Zr+Nb+Ce+Y–Na<sub>2</sub>O+K<sub>2</sub>O/CaO plot of [102]. (G) Y+Nb–Rb plot of [103]. L–P: low peraluminous; m–P: moderately peraluminous; h–P: highly peraluminous; f–P: felsic peraluminous; FG: fractionated felsic granites; OGT: M-, I-, and S-type granites; syn-COLG: syncollisional granites; WPG: within plate granites; VAG: volcanic arc granites; ORG: ocean ridge granites.



<b>Nb-Ta-rich granites</b>		<b>Nb-Ta-poor granites</b>	
◆ Penouta (Sn-Ta-Nb±Be)	▲ Acebo (Li-W±Nb)	▽ Ponte Segade (W±Nb±Ta)	▽ Laza (Sn±Ta)
■ Golpejas (Sn-Ta-Nb±Li)	◇ Belvis de Monroy (Be±Li)	⊗ Beariz (Sn±Nb±Ta)	○ Jálama (Li±Nb)
■ Argemela (Li-Sn-Ta-Nb)	★ Fuentes de Oñoro (Li-Sn-Ta-Nb)	▽ Logrosán (Sn±Nb)	☆ Fontao (W±Sn±Nb)
■ Tres Arroyos (W-Li-Nb-Ta)	★ El Trasquilón (Sn-Li±Nb±Ta)	◇ Pedroso de Acim (W-Sn-Li±Ta)	

Figure 4. Variation diagrams for major elements (A–F).

With respect to the variation diagrams, the sum of Fe, Mg, and Ti (Figure 4) has been used as a marker of evolution instead of silica to avoid the effect of fluxing elements on the equilibrium of quartz and albite. Most of them were scattered, but certain trends can be observed. Thus,  $K_2O$  as a whole tended to decrease with evolution, which is more pronounced in Nb-Ta-rich granites (Figure 4D).  $Na_2O$  showed an increase with evolution in Nb-Ta-poor granites, while the increase was more significant in Nb-Ta-rich granites (Figure 4C). Silica showed a clear dual behavior depending on the granitic type, with a tendency to increase in Nb-Ta-poor granites and to decrease in Nb-Ta-rich granites (Figure 4A). Al showed considerable scatter, although Nb-Ta-rich granites tended to have higher contents (Figure 4B). Ca and P showed no clear evolutionary patterns in most plutons, except for the Nb-Ta-rich granite plutons of Belvis and Fontao, where P tended to increase and Ca tended to decrease with evolution. (Figure 4E,F). In addition, Nb-Ta-rich granites tended to be richer in Ca, probably because of their higher apatite content, which is consistent with their high P abundance.

### 5.2.2. Trace Element and REE Concentrations

In the Iberian rare metal granites, the HFSE, namely Zr, Hf, Ta, Sn, Nb, U, W, and REE, are strongly controlled by accessory minerals. In this regard, the columbite group minerals of Nb-Ta-rich granites were shown to host Nb and Ta, with high Ta contents in the Villardecievros (up to 273 ppm), Penouta (up to 226 ppm), and Golpejas (up to 215 ppm) granites (Tables 1 and 2). The Nb/Ta ratio was rather low (average 1.4), with the highest values in the Nb-Ta-poor granites (close to 7 in the Logrosán granite), where CGM are absent, and values  $< 2$  in the Nb-Ta-rich granites, where CGM are present (Figure 5).

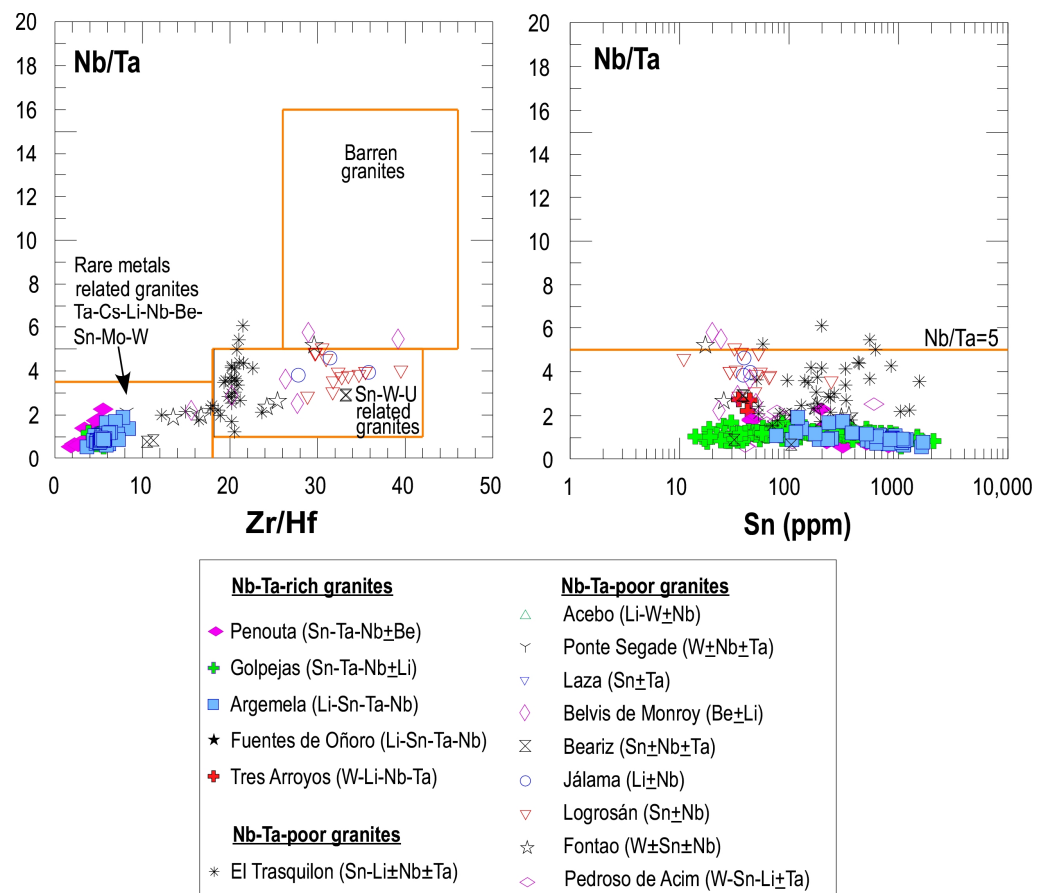


Figure 5. Evolution of Nb/Ta ratio as a function of Zr/Hf and Sn (from [107]).

Sn was mainly hosted in cassiterite and to a lesser extent in stannite and varlamoffite. Sn was highly enriched in the greisen or quartz veins of Sn granites (up to 7201 ppm) and

showed values up to 3800 ppm as disseminated mineralization in Nb-Ta-rich granites (e.g., Penouta), although the latter also showed low values (20 ppm in Golpejas) (Figure 5).

Zirconium was mostly hosted in zircon and to a lesser extent in CGM. This element was high in the Nb-Ta-poor granites (up to 118 ppm in the Logrosán granite see Table 2) and distinctly low in the Nb-Ta-rich granites, with values up to 39 ppm measured in the Golpejas granite and as low as 10 ppm measured in the Argemela granite (Figure 5 and see Table 2). On the contrary, the Hf values (also hosted in zircon) were high in the Nb-Ta-rich granites (up to 8.5 ppm measured in the Penouta granite) and typically low in the Nb-Ta-poor granites (maximum value of 3.1 ppm measured in the Logrosán granite) (see Table 2). Regarding the Zr/Hf ratio, there was a clear contrast between Nb-Ta-poor granites, with values greater than 10, and Nb-Ta-rich granites, with values less than 8 (Figure 5), mainly because the latter were found to be richer in Hf. U abundance (50–0.7 ppm, average 11 ppm) was higher than in the mean upper crust, with the Clarke value (av. 2.7 ppm) indicating a “fertile” source of U. The highest U contents were found in the El Trasquilón (up to 50 ppm) and the lowest in the Logrosán granite (Table 2).

It should be stressed that there was a high measured abundance in certain LILE elements, especially Rb (up to 2448 ppm, average 920 ppm, and with the highest values in the Nb-Ta-rich granites of the Argemela granite, Table 2), Cs (up to 350 ppm in the Argemela granite, average 57 ppm; Table 2), and Sr (up to 677 ppm in the border facies of Argemela, average 39 ppm, Table 2). The high Ga contents are noteworthy (Table 2), especially in the Nb-Ta-rich granites, (up to 329 ppm in the Golpejas granite). Li contents were significantly high in the granites of Fuentes de Oñoro (8300 ppm), Argemela (5532 ppm), and El Trasquilón (4555 ppm). The Golpejas granite had low Li (86 ppm on average, maximum of 1084 ppm, Table 2), but with intragranitic veins rich in montebrasite. It should be noted that Be was present in significant amounts, as in the Argemela granite (up to 385 ppm), Penouta (up to 125 ppm), the Golpejas granite (up to 103 ppm), and the Beariz granite (up to 91 ppm), which according to [108], would be Be-bearing granites.

Fluorine data are scarce, but some Nb-Ta-rich granites, such as the Golpejas and Argemela granites, were found to reach up to 1.6% and 1.3%, respectively, and always with lower values in the Nb-Ta-poor granites (up to 0.58% in the El Trasquilón granite) (Table 2).

Upper crust normalized patterns of Nb-Ta-rich granites displayed positive peaks in Rb, U, Ta, Nb, Hf, and occasionally in some REE (Gd, Tg, Dy, and Ho) and negative anomalies in Ba, Th, La, Ce, Pr, Nd, and Ti (Figure 6). In contrast, the Nb-Ta-poor granites (e.g., Logrosán, and Fontao) showed positive peaks in Rb, U, Ta, and sometimes in some REE, and negative anomalies in Ba, Th, Sr, Eu, Ti, La, and Ce. It is worth noting that the REE content was usually lower than the upper crust content (Figure 6).

The REE patterns were variable (Figure 8) in the Nb-Ta-rich granites, with typical M-shaped tetrad patterns in the Penouta granite and very irregular patterns in the Golpejas and Argemela granites, in addition to low REE contents and a distinct tetrad effect in most of them (Figure 8). In contrast, the Nb-Ta-poor granites exhibited more uniform geometries, a pronounced Eu anomaly, and a low tetrad effect (Figure 8). The  $\Sigma$ REE content was distinctly low in the Nb-Ta-rich granites (up to 0.08 ppm in the Golpejas granite), with values increasing in the Nb-Ta-poor granites (up to 117 ppm in the Logrosán granite) (Table 2). The REE fractionation  $(La/Yb)_N$  was generally low, being higher in the Nb-Ta-poor granites (up to 33 in the Logrosán granite) than in the Nb-Ta-rich granites (up to 0.03 in the Argemela granite). Most samples showed a weak negative Eu anomaly ( $Eu/Eu^*$  average of 0.46), with an occasional positive Europium anomaly ( $Eu/Eu^* = 1.94$  in the border facies of the Argemela granite).

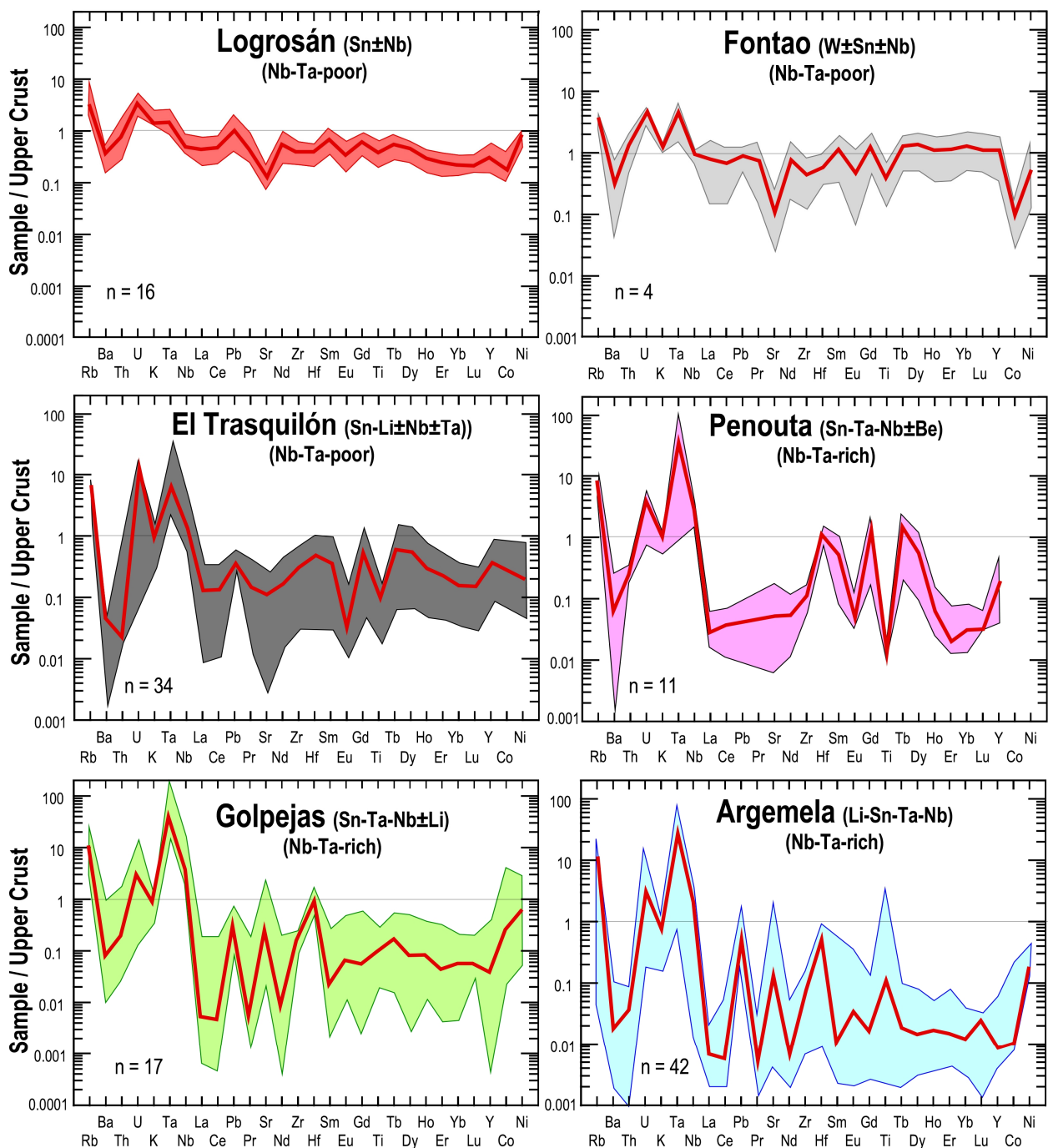


**Figure 6.** Spidergrams normalized to the upper crust from [109,110]. The thick red line represents the mean normalized value. The number of data (n) is also included.

### 5.2.3. Isovalent Trace Element Ratios and Lanthanide Tetrad Effect ( $TE_{1,3}$ )

Typical isovalent trace elements such as Zr, Hf, Y, and Ho, as well as the lanthanide tetrad effect were used to decipher whether geochemical twins such as Zr-Hf and Y-Ho showed chondritic ratios (CHARAC behavior) typical of pure silicate melts or non-chondritic behavior as a result of fractionation in aqueous media or in high-silica magmatic systems enriched in water, Li, B, F, P, and Cl [111]. These geochemical twins were also compared with the Nb/Ta ratio, which is typical of pure magmatic systems with values higher than five [107].

The Zr/Hf ratio varied widely between the Nb-Ta-poor granites, where it was found to be chondritic, and the Nb-Ta-rich granites, which all had subchondritic values (Figure 7).

In the Nb-Ta-poor granites, although the Zr/Hf ratio varied widely, there was little tetrad effect, and the Y/Ho ratio varied little, which was chondritic. However, in the Nb-Ta-rich granites, the Y/Ho ratio and the tetrad effect had a very large range of variation, with a limited Zr/Hf ratio. On the other hand, the Nb/Ta ratio tended to behave analogously to the Zr/Hf ratio, with a very significant variation in the Nb-Ta-poor granites and a much less pronounced variation in the Nb-Ta-rich granites.

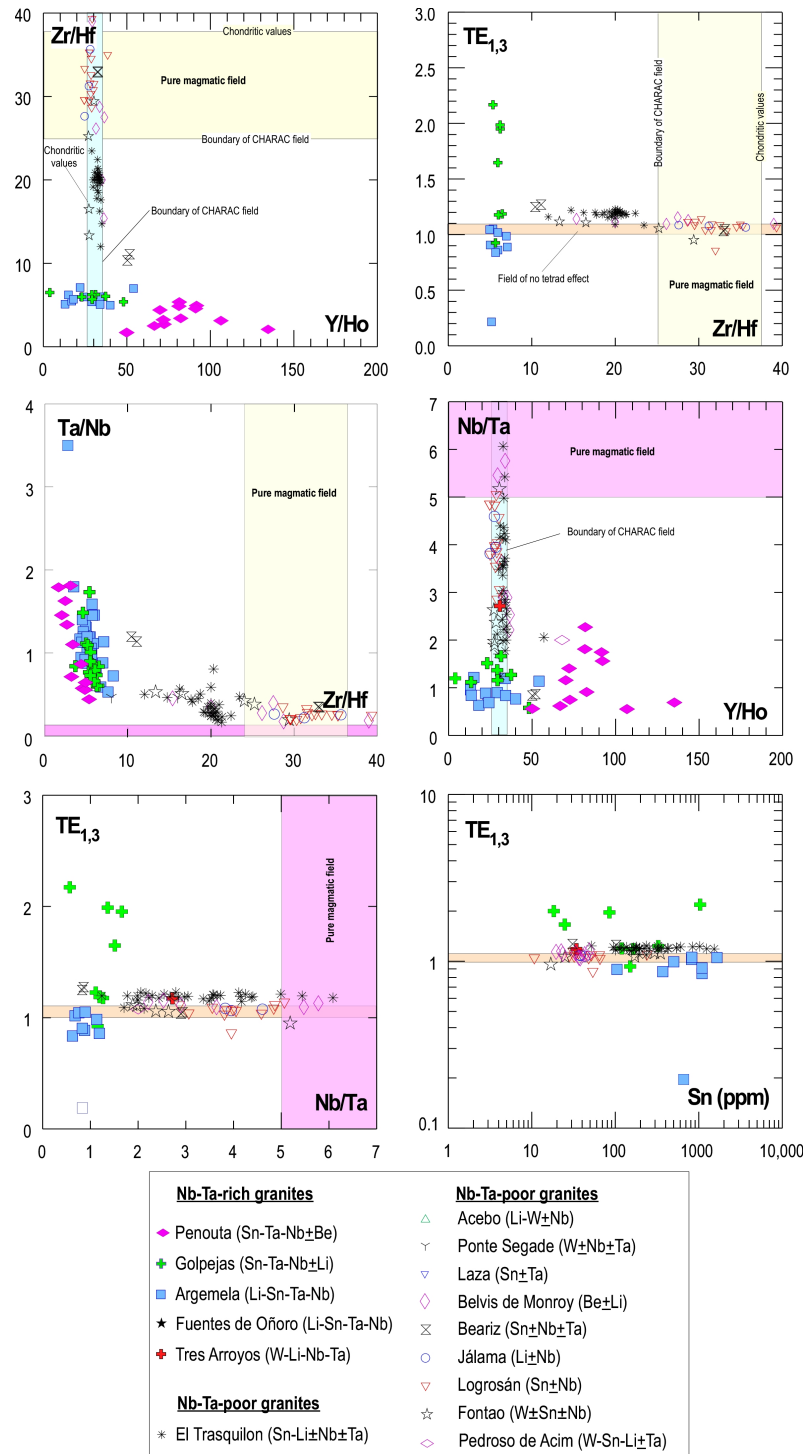


**Figure 7.** Binary plots showing ratios of isovalent trace element ratios and lanthanide tetrad effect ( $TE_{1,3}$ ). The colored areas indicate domains of granitic melt evolution with little or no fluxing elements. The fields were constructed following [107,113].

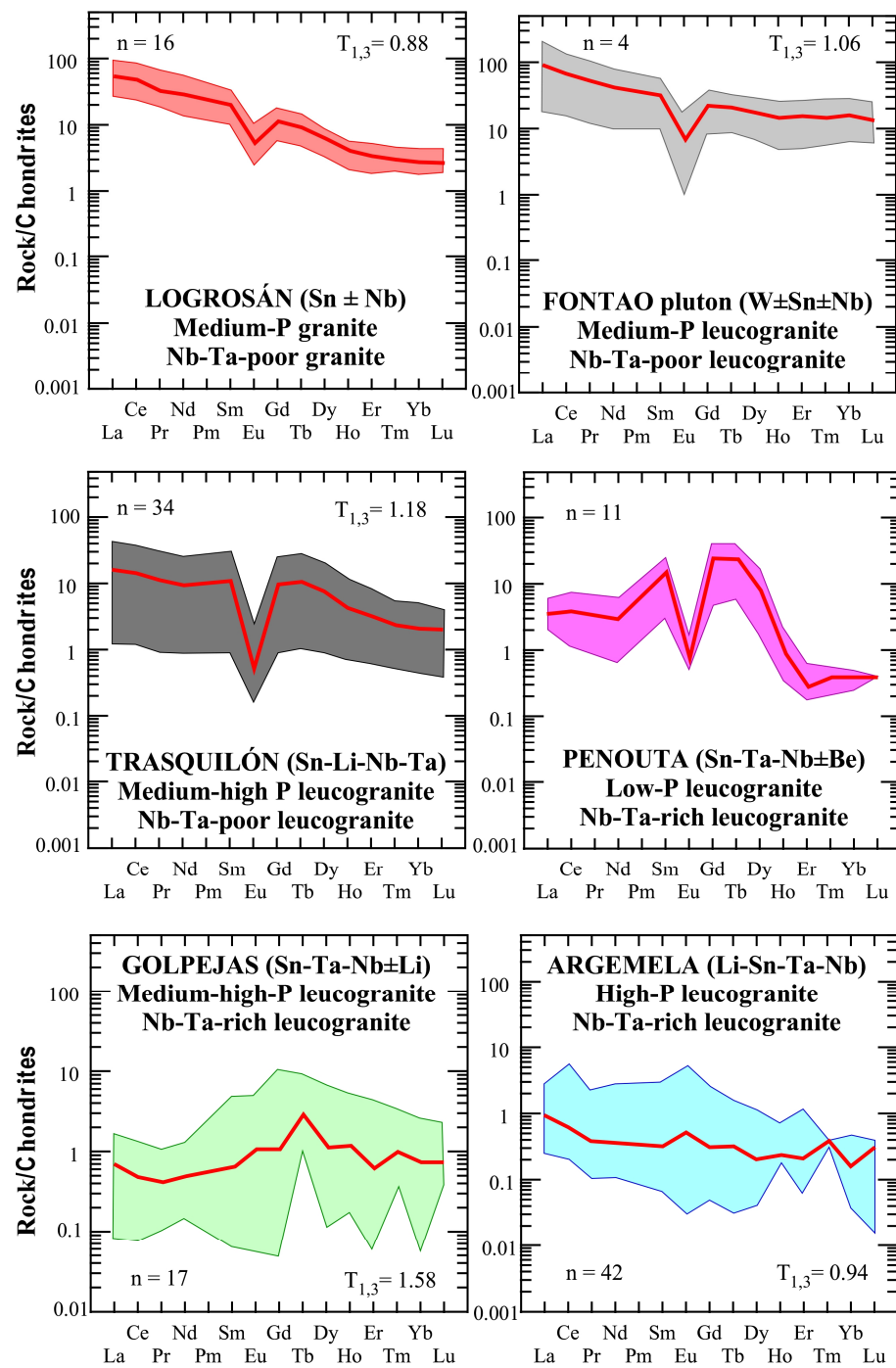


**Figure 8.** REE patterns normalized to the chondrite from [112]. The thick red line represents the mean normalized value. Tetrad effect ( $T_{1,3}$ ) from [113] and number of data ( $n$ ) are also included.

Taking into account the values of chondrites, the limits of the CHARAC field, the field of no tetrad effect, and the limit of the magmatic–hydrothermal environment as pertains to the Nb/Ta ratio (Figure 7), it is confirmed that that Nb-Ta-poor granites can be attributed to granitic melts following an evolution with little or no participation of fluxing elements. In contrast, the geochemical signature of the isoivalent trace element ratios and the lanthanide tetrad effect of the Nb-Ta-rich granites are typical of a melt with an abundance of fluxing elements and with an important evolution in the magmatic–hydrothermal transition (see [107,111,113]).

### 5.2.4. Isotope Geochemistry

Isotopic data from Iberian RMGs are very scarce; only Sr-Nd data are available from granites from the central and southern part of the Central Iberian Zone, specifically from the plutons of Sn-Nb from Logrosán [54], Be±Li from Belvis de Monroy [82], and W-Li-Nb-Ta from Tres Arroyos [114]. The Logrosán granite showed a large variation in the initial  $^{87}\text{Sr}/^{86}\text{Sr}$  ratios (0.7125–0.7286) and a restricted  $\epsilon\text{Nd}$  (−4.0 to −4.3) (Figure 9). The Belvis de Monroy (border unit) also showed a restricted range of variation in  $\epsilon\text{Nd}$  (−5.34 to −6.18) and  $^{87}\text{Sr}/^{86}\text{Sr}$  ratios (0.7074–0.7215) (Figure 9). The Tres Arroyos granite showed limited ranges of variation in  $\epsilon\text{Nd}$  (−3.42 to −5.17) and the  $^{87}\text{Sr}/^{86}\text{Sr}$  ratio (0.7125–0.7286) (Figure 9). All these values were quite similar to the host rock of these granites, i.e., the Schist Greywacke Complex.

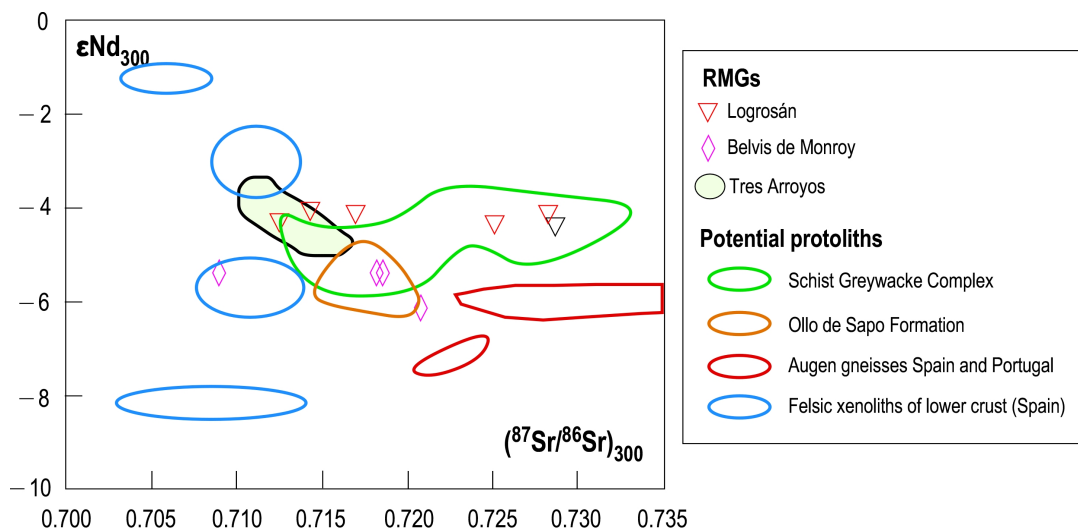


**Figure 9.** Sr-Nd diagram normalized to 300 Ma showing the isotope signature of the Logrosán [54], Belvis de Monroy (border unit; [82]), and Tres Arroyos (a unit of the Nisa-Alburquerque pluton; [114]) plutons. Potential protoliths are also included for comparison (see compilation of [54,115] and references therein).

### 5.3. Geothermobarometry

Geothermometric estimates of zircon, monazite, and apatite saturation are shown in binary plots (Figure 10). There was only a good positive correlation between the saturation temperatures of zircon and monazite, and not in all cases. The Nb-Ta-poor granites correlated in almost all cases, thus matching the 1:1 line in Figure 10, while the Nb-Ta-poor granites deviated almost systematically from this line, with the exception of the P-poor Penouta granite. The apatite saturation model shows in many cases either very high (up to >1000 °C) or very low temperatures (close to 250 °C; Figure 10), which are outside the commonly accepted temperature ranges for the crystallization of haplogranite melts (700–800 °C, see [87–89]) and rare metal magmas (around 650 °C, see [116]). The latter suggests that, in general, this thermometer was not working properly in most of our samples, perhaps because highly peraluminous, low Ca, low temperature melts are accommodating phosphorus in aluminum phosphates and/or feldspars, via berlinite substitution, rather than in apatite [95,117]. It is worth noting that the monazite saturation temperatures were too low in the phosphorus-rich Nb-Ta-rich granites, probably because there is no evidence of monazite in these granites [64,86], which was the opposite of what happened in the P-poor Nb-Ta-rich granite from Penouta [2], which showed temperatures similar to those of zircon.

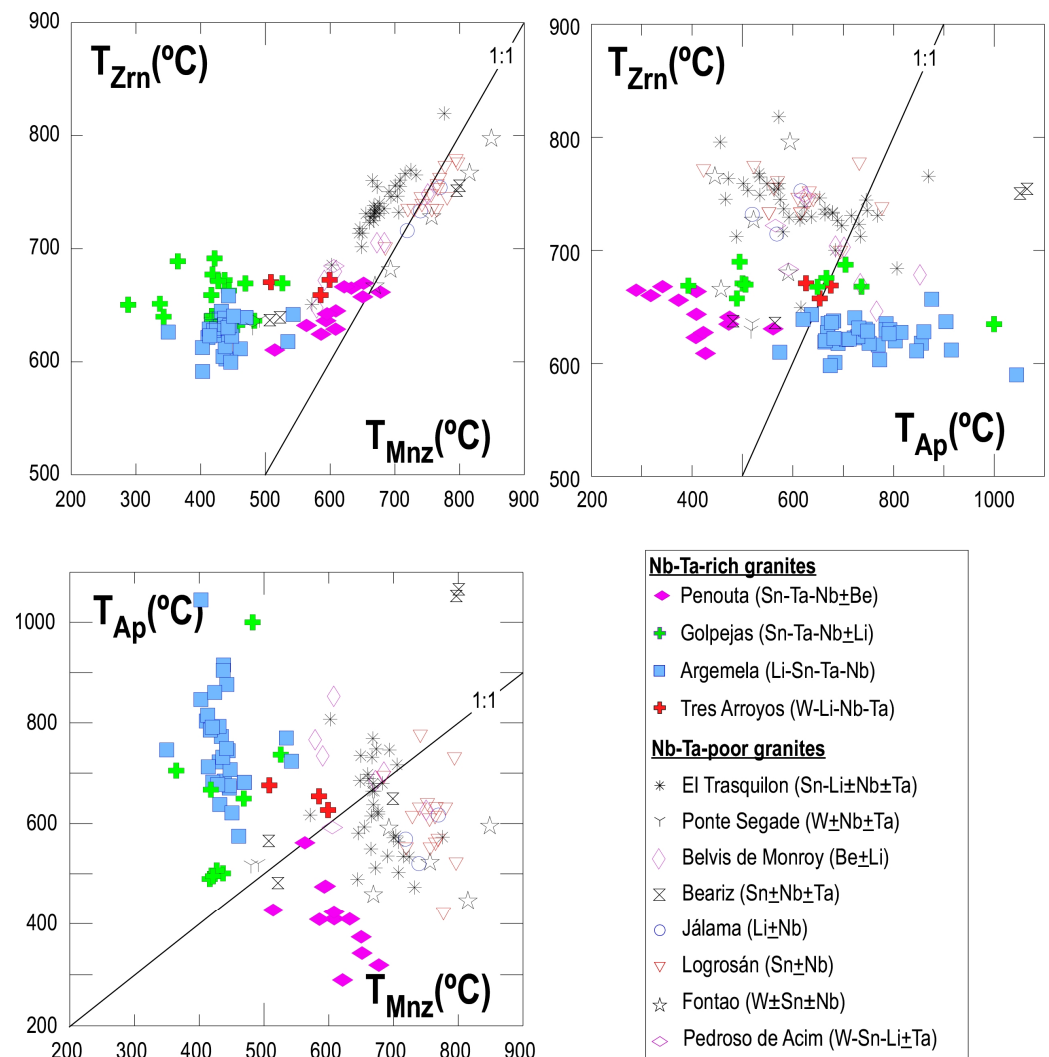


**Figure 10.** Zircon, apatite, and monazite saturation temperatures calculated based on the methods of [87–89], respectively.

Having made these observations and considering only the saturation thermometer of zircon and monazite when there was evidence of their presence in the granite, it should be noted that the Nb-Ta-poor granites were emplaced between 800 and 700 °C, while the Nb-Ta-rich granites were emplaced at a lower temperature (<700 °C), reaching values as low as 600 °C, which are quite similar to those reported for other Nb-Ta-rich granites, such as the Beauvoir granite from experimental approaches [116].

The geobarometry of these deposits is not straightforward due to the lack of suitable mineral associations. The exception could be the geobarometer using the chemistry of white mica (Si content of phengite, [90]). However, the results obtained for both phengite and muscovite white micas showed variation ranges of more than 5 kbar for each deposit in primary white micas, which is the reason for not including the results. The reasons for these not very robust results may be as follows (see [90]): not all mineral phases that are limiting associations, such as phlogopite, are present in RMG, and the white mica was in many cases muscovite and not phengite. It was decided to take into account the microthermometry reported for some of these deposits [54,118] and to consider the trapping conditions of the first fluid of these deposits, especially for the formation of quartz in equilibrium with cassiterite, as a minimum emplacement value. This first fluid in the Nb-Ta-rich granites consisted of CO<sub>2</sub>-aqueous (H<sub>2</sub>O-NaCl-CO<sub>2</sub>-N<sub>2</sub>-H<sub>2</sub>S), CO<sub>2</sub> (CO<sub>2</sub>-CH<sub>4</sub>-N<sub>2</sub>-H<sub>2</sub>S), and low-salinity aqueous (H<sub>2</sub>O-NaCl) fluid inclusions [118], whereas in the Nb-Ta-poor granites, the available data indicated N<sub>2</sub>-CH<sub>4</sub>-aqueous and low-salinity fluid inclusions [54]. Pressure

constraints from the microthermometry indicate that these granites were emplaced shallow (<3 kbar, Figure 11), especially the Nb-Ta-rich granites (<2 kbar).

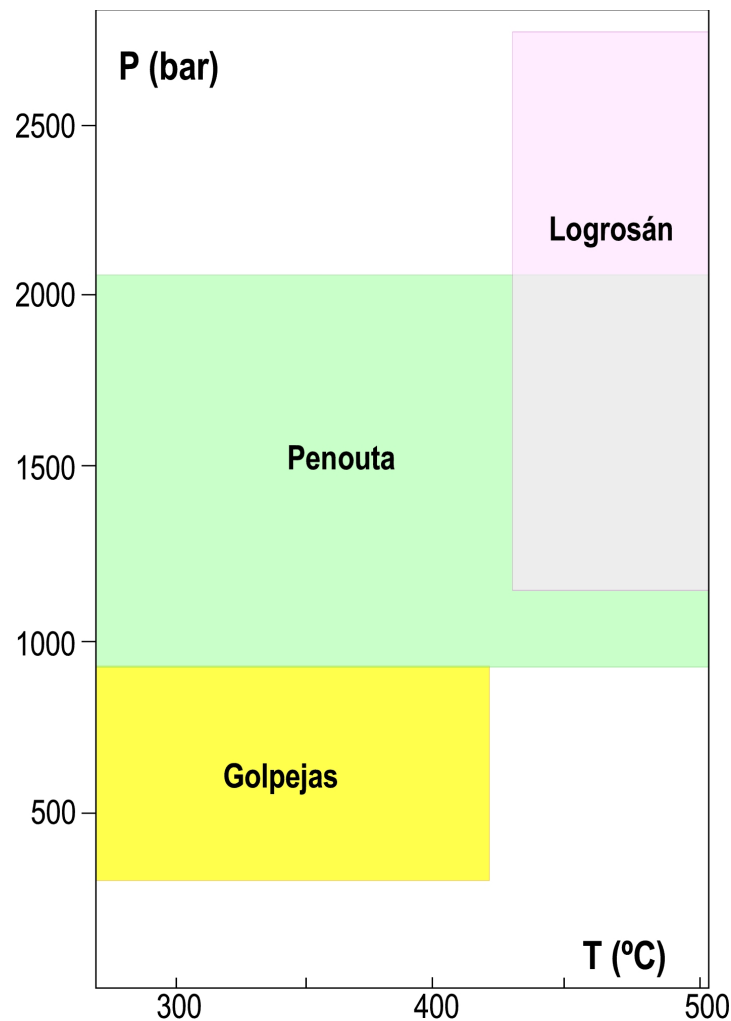


**Figure 11.** P-T reconstruction for trapping of the earliest fluids (cassiterite precipitation) in Nb-Ta-poor granites (Logrosán) and Nb-Ta-rich granites (Penouta and Golpejas). Penouta and Golpejas conditions from [118] and Logrosán estimates from [54].

#### 5.4. Water Content

$H_2O$  (vapor) =  $H_2O$  (melt) equilibrium showed high  $H_2O$  contents in the rare metal granites, with values close to 6% for the shallow cooling conditions of these granites. It is noteworthy that the Nb-Ta-rich granites had higher  $H_2O$  contents than the Nb-Ta-poor granites (Figure 12A,B).

Considering isobaric cooling (Figure 12A), the  $H_2O$  content increased slightly up to temperatures close to 600 °C, i.e., close to the solidus, and then decreased. When the melt evolved by isothermal decompression, a loss of water in the melt was observed as the confining pressure decreased (Figure 12B). This behavior can lead to the separation of the fluid phase first by boiling [119,120]. With the isothermal decompression, water loss was more pronounced than with the isobaric cooling at temperatures near the solidus. (Figure 12B).

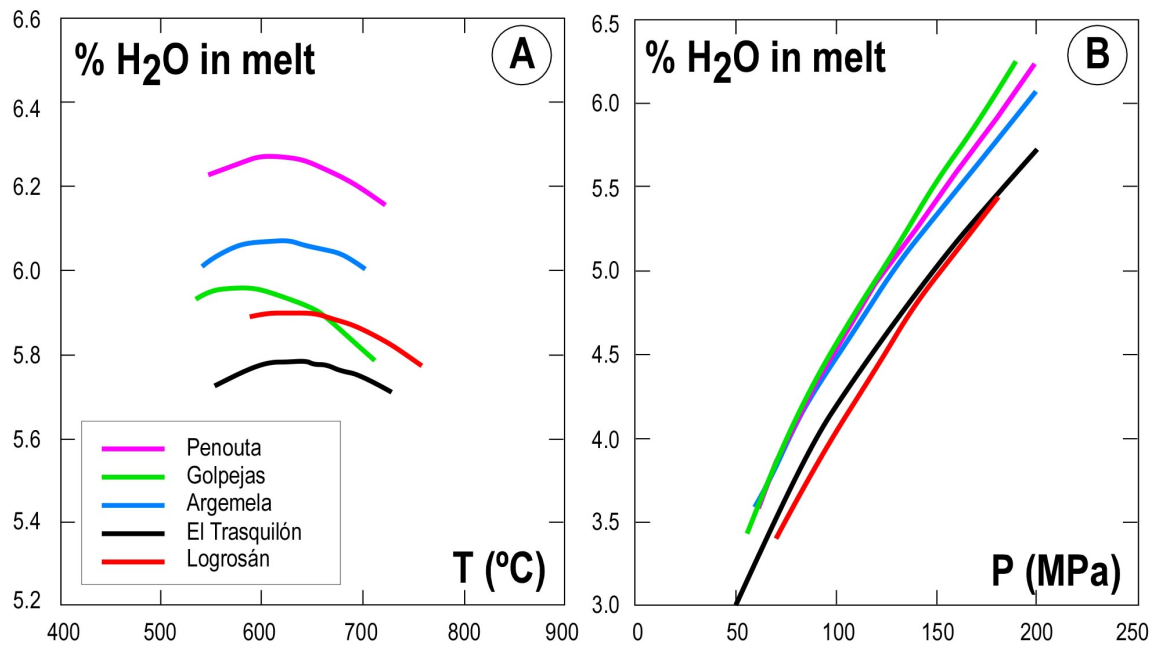


**Figure 12.** Melt water content versus temperature (A) and pressure (B) in selected rare metal granites. Pressure in A ranges from 100 MPa (Golpejas) to 200 MPa (the others). The temperatures used in B are those of zircon saturation (averages): 666 °C (Penouta), 670 °C (Golpejas), 637 °C (Argemela), 716 °C (El Trasquilón), and 782 °C (Logrosán).

## 6. Discussion

### 6.1. The Source and the Parental Magmas of Iberian Rare Metal Granites

The source of the Iberian RMG is poorly known and has only been addressed in those cases where isotopic data are available, specifically in three granites (Figure 9): two of them poor in Nb-Ta (Logrosán and Belvis de Monroy) and one rich in Nb-Ta (Tres Arroyos). For these granites, a derivation from Neoproterozoic sequences, and particularly from the Schist Greywacke Complex, has been inferred. This conclusion is supported by a range of initial isotopic (Sr, Nd) ratios similar to those measured in the granitoids (Figure 9) and by the high phosphorus concentrations in both the metasediments and these granites [54,81,114,121]. However, Figure 9 shows that lower crustal augen gneisses and eventually felsic xenoliths also have similar Sr and Nd ratios to RMGs. Similarly, some authors point out that the isotopic signature may be strongly influenced by partial melting of the source rock, which may mobilize melts with isotopic and geochemical fingerprints that are different from the restitic material and, thus, from the bulk rock composition of the locally exposed protoliths [122–126]. This could make it difficult to determine the source area of the RMGs based on their isotopic signatures alone. Recently, in the French Massif Central and by means of thermodynamic modeling, a felsic metaigneous source has been suggested as the most favorable protolith to produce Li-F-rich peraluminous granites [127], like many of the Iberian RMGs, which opens the possibility to also investigate this type of protolith in Iberia as a source of the Iberian RMGs.

The Iberian rare metal granites, like other rare metal granites worldwide, have a composition that has been explained by a process of extreme differentiation (e.g., [128]), melts from special protoliths plus fractional crystallization [6,127,129], and metasomatic processes [61,130,131]. The metasomatic processes that link the chemistry of the RMGs to the destabilization processes of the biotite and feldspar from deeper zones are now questioned by the existence of volcanic/subvolcanic equivalents (ongonites and macusanites [132–135]) with identical compositions to the RMGs, the existence of experimental work that reproduces the chemistry of these granites from melts enriched in fluxing elements [95,116,135], and the existence of melt inclusion with this geochemistry [136]. While it is true that many of the rare metal granites show evidence of hydrothermal activity, this is more related to the

evolution of the magma at the emplacement site (see below) than to fluids of a deep origin. The possibility that these granites are derived from specialized protoliths is attractive, because they require a smaller volume melting process and less fractionation to achieve the same level of enrichment compared to unenriched protoliths [137]. However, to achieve the high enrichments of rare metal granites, an extensive fractional crystallization process is required.

Most of the Iberian rare metal granites were found to occur in isolated bodies with no apparent spatial relationship with other less-evolved granites (Penouta, Golpejas, Argemela, El Trasmilón, Logrosán, Ponte Segade, Laza-Arcucelos, Pedroso de Acim, Belvis de Monroy, and Acebo), which could indicate that there is no direct relationship with a less evolved parental magma. However, there were cases, such as the granites of Fuentes de Oñoro or Villardeciervos, where they were found to be spatially associated with less evolved granites. Likewise, gravimetric surveys carried out in the Logrosán granite [54] and the existence of deep boreholes in the Golpejas [86] seem to confirm that there are less evolved granites at depths that could represent the parental magmas of these granites, thereby reinforcing the hypothesis that RMGs are formed by a process of extreme differentiation.

A process of extreme differentiation from nearby granites has also been invoked to explain the genesis of Iberian aplites and LCT pegmatites [31]. Indeed, these authors find geochemical affinities, especially in trace elements, between LCT pegmatites and two granite suites: two-mica granites and P-rich and highly peraluminous granites. From Figure 13, it follows that there could also be geochemical affinities between RMGs and different types of Iberian granites, which is in line with the evolutionary trends postulated by [31]. The geochemical affinity is mostly with two-mica granites and P-rich and highly peraluminous granites in a similar fashion that LCT pegmatites, although eventually with granodiorites (Penouta granite) (Figure 13). The latter supports the notion that most Iberian RMGs could be derived from two-mica and P-rich highly peraluminous granites, perhaps excluding the Penouta granite. In addition to its affinity with granodioritic magmas, the Penouta granite has a number of distinguishing features with respect to the rest of the RMGs that should be highlighted: (i) it is the only Iberian RMG with a low phosphorus content, which could indicate a different parental magma, a different evolutionary process, or a different source; and (ii) it is the only one in which granodiorites occur in close proximity. Furthermore, mass balance modeling of major elements, as well as Rayleigh modeling with trace elements controlled by main minerals, such as Ba, Rb, and Sr (Figure 13B,D), do not seem to rule out that the Penouta granite could have a granodioritic parental magma. Nevertheless, although this is an interesting issue, further geochronological and petrogenetic work, which is beyond the scope of this paper, is needed to determine whether granodiorites can be the parental magma of the Penouta RMG.

## 6.2. Chemical Evolution in Iberian RMGs

As seen above, the RMGs appear to be derived by a process of differentiation from some surrounding granites. Having a compositional starting point allows us to address an issue that is not entirely clear for RMGs: what is their geochemical evolution in a purely magmatic system?. We have attempted to address this evolution through thermodynamic modeling with the Rhyolite-MELTS application of [92] considering as parental magma a two-mica granite, since, as seen above, it is probably the most common parental magma for the Iberian RMGs. However, the evolution obtained does not fit any of the granites considered, with a particularly poor fit for the Nb-Ta-rich granites (Figure 14). The discrepancy is due to the fact that the RMGs show an evolution to the Ab apex in Figure 14, and Rhyolite-MELTS predicts an evolution to the Qzt apex. The latter suggests that quartz saturation is underestimated by the Rhyolite-MELTS, probably because this tool does not evaluate the effect of fluorine or other fluxing elements that modify the stability field of quartz. Therefore, Rhyolite-MELTS is not a suitable tool for modeling the evolution of a parental magma to RMGs.

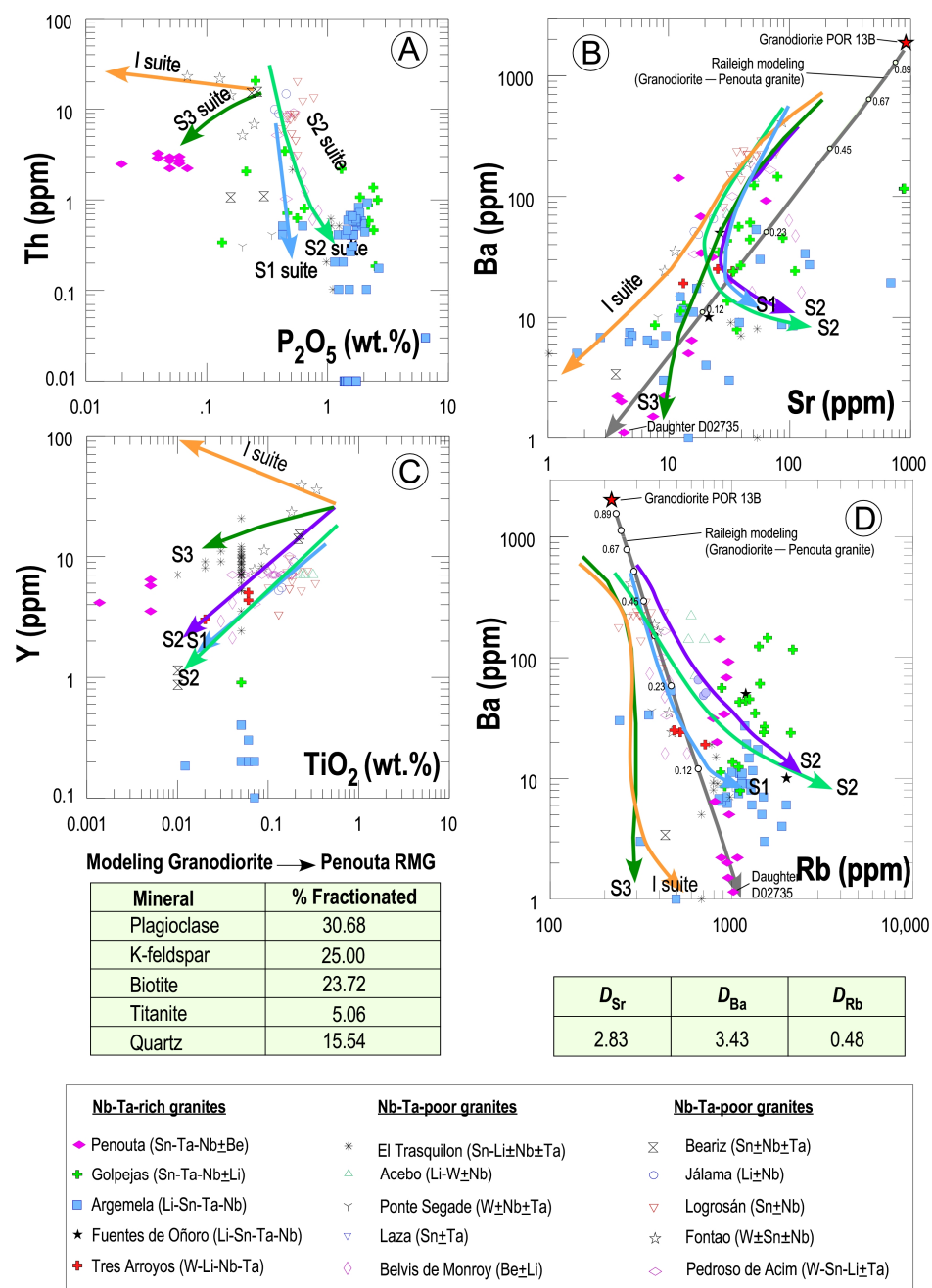


**Figure 13.** Typical chemical trends in Iberian granite suites (I suite and S1 to S3 suites) derived from CIZ granites and aplite pegmatites according to [31] in different plots (A–D). The S1 suite corresponds to the two-mica leucogranite suite, the S2 suite to the P-rich highly peraluminous granite suite, the S3 suite to the P-poor moderately peraluminous granite suite, and the I suite to the low peraluminous I-type granite suite. In (B,D), Rayleigh fractionation modeling (line in gray and also for elements controlled by main minerals, i.e., Sr, Ba, and Rb) is also included to obtain constraints on the evolution of a parent melt consisting of granodiorite POR 13B. In this modeling, the cumulate mode (table in green) was estimated using major element-based least squares modeling, thus yielding a sum of squared residuals of 0.6 for granodiorite POR 13B from the Tormes dome as parental melt and sample D02735 from the Penouta granite as daughter. Labeled ticks indicate decreasing melt fraction. Bulk  $K_d$  for Sr, Ba, and Rb are also included in the table in green. Whole rock data for parent and daughter are given in Table S3. Major element-based least squares modeling was performed using the OPTIMASBA code of [93] and Rayleigh modeling using the FC-AFC-FCA code of [94]. The partition coefficients of Sr, Ba, and Rb are taken from the compilation of [138,139].

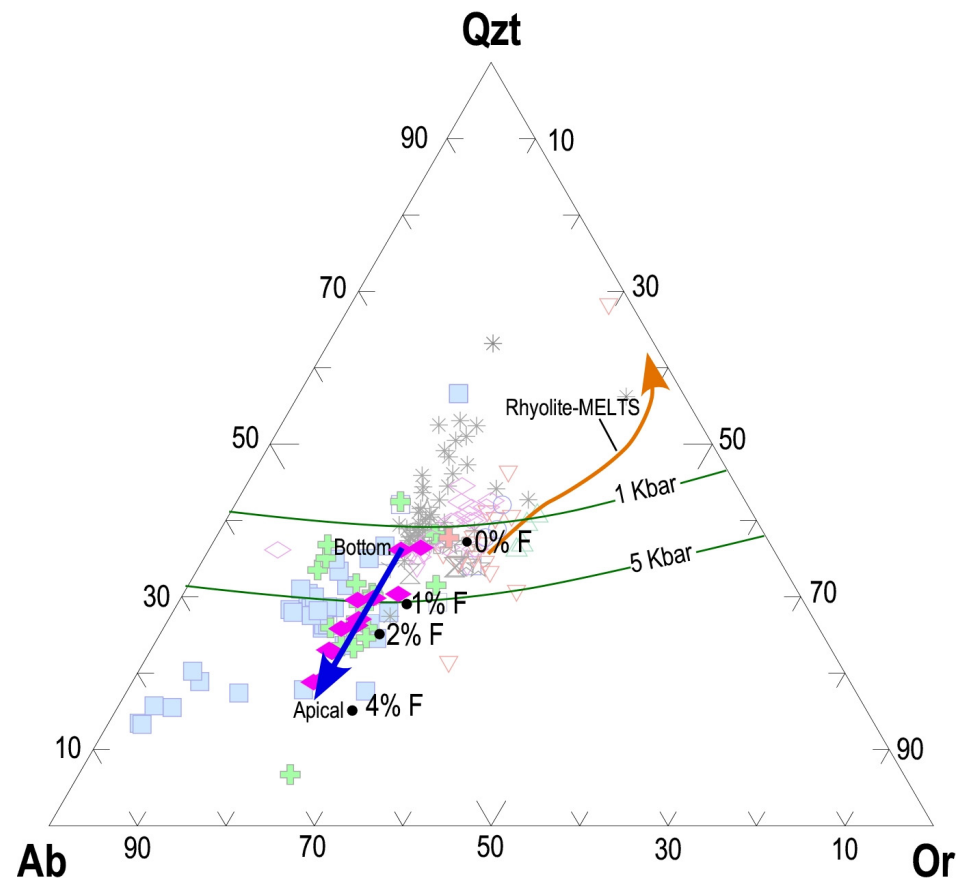


**Figure 14.** Qzt-Ab-Or plot showing normative composition of all Iberian RMGs. In the Penouta pluton is shown the variation of normative composition from bottom to top (dark blue arrow). Granite minima for a system with excess water at 1 kbar and 0, 1, 2, and 4% added fluorine is also shown, with data being from [135]. Cotectic lines for  $P(\text{H}_2\text{O})$  of 1 and 5 kbar (green lines) are taken from [140]. Rhyolite-MELTS simulation for a two-mica granite as parental melt (sample DTI-11 after [141]), a pressure of 2 kbar, 2% of water content, and oxygen fugacity buffered at FMQ. Symbols as in Figure 13.

Looking at the variation diagrams (Figure 4), one of the most striking aspects in the RMGs' evolution, especially those rich in Nb-Ta, is the strong enrichment in Na in some samples, accompanied by decreases in Si and K and increases in Al, resulting in melts with a significant increase in normative albite (Figure 14). At the pluton scale, this enrichment in Ab normative usually occurs in the apical zones, as occurred in the Penouta granite (Figure 14), and can be explained as follows: (i) the presence of fluxing elements, such as fluorine, in the system that modify the stability of quartz [135]; (ii) a superimposed albitization process; (iii) a combination of both processes; or (iv) undercooling disequilibrium crystallization [142]. Analyses of the fluxing elements in the Iberian RMGs are scarce, and those available (0.3% average F, maximum 1.6% in Golpejas; 0.1% average F, maximum of 0.5% in Logrosán, Table 2) do not reach the high fluoride contents necessary to significantly increase the stability field of quartz (2–4%, Figure 14 and see [135]) and produce albite-rich melts via flux-rich melts. In some cases, such as the Golpejas and the El Tráquilón granites, some of this fluoride could have been removed from the magma by an exsolved fluid phase, since the deposits have montebasite-rich veins [74,86]. However, there are cases, such as the Penouta granite, where this fluoride loss is not so easy to explain due to the absence of montebasite and the extremely low amount of apatite [2]. Recent work analyzing the metasomatism produced by Li-bearing pegmatites and aplites in their metamorphic host shows that significant concentrations of fluxing elements (Li and F) were able to leave the melt and be incorporated into their host rock [143]. This fact could suggest that the

evolution of RMG melts could have occurred with high fluxing element contents. The existence of saturation and exsolution processes of the volatile phase, see below, could have scavenged the fluxing elements from the residual melt, thereby resulting in its present impoverished signature. The available fluoride data seem to indicate that the Nb-Ta-rich granites have significantly higher fluoride contents than the Nb-Ta-poor granites, where Na enrichment is not as pronounced. It is consistent with the importance of fluorine in melt evolution to the albite-rich granites.

Moreover, the presence of alkali feldspars corroded by albite and two-albite generations is the rule in RMGs, especially in the Nb-Ta-rich ones [2,61], and it seems plausible that a superimposed albitization process enhanced albite formation and also induced Na enrichment of the RMGs, namely the Nb-Ta-rich ones.

In addition, severe undercooling, as may have occurred in the sheet-like granites of limited thickness such as Golpejas, could lead to isothermal subsolidus fractional crystallization and localized feldspar enrichment. In this scenario, a melt may remain metastable at temperatures below its thermodynamic solidus before crystallization begins [142]. In this situation, the mineral with the highest chemical potential in this undercooled state crystallizes first. In granitic pegmatites, the alkali feldspar would crystallize first, thus leaving the quartz for later [142]. This would result in a higher amount of alkali feldspar in the areas of greater undercooling, such as the margins, and a higher proportion of quartz in the core, which crystallizes later. In the Golpejas granite, one of its margins is highly kaolinized and cannot give us much information. However, the other margin is fresh and shows a significantly higher amount of alkali feldspar than the core, which could indicate that disequilibrium crystallization may play an important role in the evolution of these thin bodies.

### 6.3. The Role of Fluids in the Crystallization of Iberian RMGs

The intensive variables, as well as some geochemical and textural features of the Iberian RMGs, suggest that these granites may have undergone fluid phase exsolution and, in some cases, may have enhanced the rare metal grades to economic levels. The high-water content of these granites, up to 6% in quite shallow conditions (Figure 12), is a critical factor in reaching saturation and causing the separation of the fluid phase at an early stage relative to the crystallization progress [119]. In general, early saturation allows ore elements to be incorporated into the volatile phase from the outset, which is something that does not occur in undersaturated magmas, where ore elements can become part of the magmatic minerals, thus reducing the amount of ore elements that could pass into the volatile phase when saturation occurs [144].

There are two other mechanisms that allow the liquid phase to exsolve: isothermal decompression and isobaric cooling with the crystallization of anhydrous phases. In an isothermal decompression scenario, the rise of a magma at lower pressures causes the amount of water dissolved in the melt to decrease dramatically (Figure 12B), thus favoring the saturation and exsolution of the fluid phase (first boiling). The low pressures estimated in the Iberian RMGs, especially those rich in Nb-Ta (<2 kbar), suggest that isothermal decompression processes most likely occurred in the Iberian RMGs. The isobaric cooling mechanism (Figure 12A) is also very feasible, because most of the crystallizing minerals are anhydrous (modal contents of hydrated minerals were only of about 10% in Penouta and Argemela [2,64]). This essentially anhydrous crystallization increases the volatile content in the melt until a point is reached at which the melt becomes saturated, and the liquid is exsolved (second boiling), which is particularly easy in the shallower environments (e.g., Golpejas granite). Second boiling may be increased by strong undercooling, especially in the border zones of the granite in contact with the colder host rock. This phenomenon has been described in the lenticular granite of Penouta, both in the wall and roof zones, where volatile phase exsolution has been associated [2], thus explaining the highest Sn contents in the apical zone and the core of the granite body. It is quite probable that this phenomenon also occurred in the tabular granite of Golpejas, which, due to its re-

duced thickness (maximum 30 m), must have been strongly undercooled in its apical and basal zones.

At the mesoscopic scale, we also find evidence of volatile phase saturation processes in the Iberian RMGs, such as the presence of greisen (Penouta, Golpejas), as well as pegmatites interbedded with aplites in the apical part of the granite (e.g., Penouta, [2]). Also at the microscopic scale, the presence of snowball quartz with plagioclase microinclusions has been associated with the presence of an exsolved fluid phase [145], which could have occurred in the Golpejas, Penouta, and Argemela RMGs.

Whole rock geochemistry also seems to support that the melt of the Nb-Ta-rich Iberian RMGs crystallized in a volatile-rich aqueous environment. Indeed, twinned elements such as Zr-Hf, Y-Ho, and Nb-Ta showed values far from chondrite (Figure 7) by fractionation in a fluid-rich environment, probably with an abundance of fluxing elements and with an important evolution in the magmatic–hydrothermal transition [107,111,113].

Similarly, geothermometric constraints from the Golpejas granite also seem to support the involvement of a fluid phase at temperatures below the granite solidus, as shown by Kfs–plagioclase and muscovite–plagioclase thermometers [146]. This fluid phase also seems to be responsible for the release of P (see Figure 2C,D), Ca, and Na, among other elements, from the alkali feldspars, thereby resulting in the strong enrichment of apatite and phosphates of Al and possibly the formation of albitites in this granite. The strong P<sub>2</sub>O<sub>5</sub> depletion calculated in the Argemela granite (Figure 2C) could also be interpreted in a similar way [59]. On the other hand, the P in the melt calculated at Golpejas highlights the possibility of filter pressing processes. The latter would mobilize P from the melt upward near the solidus if the P in the melt is higher than the P in the whole rock (Figure 2D) [95]. It is currently believed that these filter pressing processes are assisted by exsolved fluids [147]. Thus, the Golpejas granites, with their high-water contents and low emplacement pressures, are an excellent candidate for fluid exsolution and migration of highly evolved and presumably metal-rich melts by gas-driven filter pressing processes.

#### 6.4. Ore Formation in Iberian RMGs

##### 6.4.1. Sn-Nb-Ta-Rich Granites

The Iberian Nb-Ta-rich RMGs where the ore genesis is best known are the Penouta and Argemela granites. In the Argemela granite, significant LA-ICP-MS characterization of micas and quartz has been carried out [5,59], which has made it possible to investigate the genesis of the ore from a magmatic stage to a hydrothermal event. According to [5], the evolution of the ore (Li, Sn, Nb, and Ta) is very well explained according to a magmatic model in which the saturation of accessory phases, first of montebrasite, then of cassiterite, and finally of CGMs, plays a relevant role in explaining the decrease in Li, Sn, Nb, and Ta in muscovite and in the melt itself. In contrast, the evolution of W cannot be explained by the saturation of wolframite in a magmatic system, and a magmatic fluid phase is involved to which W would migrate, since the fluid/melt partition coefficient of this element is significantly high [64].

In the Penouta granite, the crystallization of CGMs is purely magmatic, as is most of the cassiterite, which seems to be partly related to an exsolved fluid that causes the highest Sn enrichments, both in the granite (central part in association with Be) and in the metamorphic wallrock of the top, where a Sn-rich greisen is formed [2]. Based on mass balance and Rayleigh fractionation models, ref. [2] carry out a model that explains the variation in the Ta/Nb ratio from the bottom (rich in white mica) to the more Ta-enriched apical part, which is poor in white mica. In this model, white mica fractionates from the bottom to the top and plays a very important role as a fractionation phase, since this mineral fractionates more Nb than Ta [148]. In this modeling, the Nb and Ta concentrations match the real sample concentrations without considering other fractionation phases of Nb with respect to Ta, i.e., CGM. The absence of inflections in Ta and Sn in variation diagrams suggests that the saturation of tantalite and cassiterite, both crystallizing in a trapped melt, has not occurred. This late crystallization is supported by the high solubility of tantalite in

haplogranite melts with fluxing elements [149–152]. Similarly, the composition of CGM itself in the CGM quadrilateral (Figure 2B), with a majority composition in intermediate positions between columbite and tantalite, has been interpreted in the context of local supersaturation processes [3].

The role of micas in the evolution of Nb and Ta in Iberian RMGs seems to be important. The evolution of Nb and Ta largely depends on the amount and type of mica removed, according to mass balance and Rayleigh fractionation modeling performed in Figure 15. Thus, the Pedroso de Acim granite had the highest inclination in the Ta/Nb ratio, thus removing micas (biotite and white mica) in a sum of 30%. It was followed by the Penouta granite and finally by the Golpejas granite, with the lowest inclination. These last two granites fractionate only muscovite, while the Penouta granite does so to a greater extent (21% vs. 9% in the Golpejas granite), which explains its greater inclination in the Ta/Nb ratio. It should be noted that there was significant scatter in the Golpejas granite, thus suggesting the involvement of processes other than white mica fractionation, e.g., exsolved volatile phase, which distort the overall evolution.

According to experimental work [153] and geochemical studies of pegmatite source rocks [143], this exsolved fluid phase may contain significant amounts of halogens and metals: Li, F, Cl, W, Sn, Be, and Ta. The importance of these halogens is that metals can greatly increase their solubility and reach high concentrations. If for some reason these compounds lose their complexing ligands, they can precipitate and form a high-grade deposit. This has been proposed in the Shihuiyao and Abbu Dabbab rare metal granites to explain the formation of Nb-Ta oxides, cassiterite, and wolframite [154,155].

On the other hand, the existence of CGMs with sponge-like textures in the apical part of granites, such as Penouta [4], has led some authors to consider the existence of a fluid phase capable of attacking a very acid-resistant mineral such as CGM. Acidic fluids appear to mobilize more Nb than Ta [156], which opens the door to the possibility that the interaction of these fluids could explain the sponge-like textures and the existence of Ta-rich CGMs in the apical granite in addition to an upward migrating Nb-rich fluid.

Moreover, the availability of P in the melt could be a critical factor in controlling the composition of GCMs in the Iberian RMGs. At high P, Ta is more insoluble than Nb, and tantalite precipitates first [157], whereas at low P, Nb is more insoluble, and columbite crystallizes first [100,158,159]. It is evident that in P-poor RMGs such as Penouta, the CGM cores tended to be Nb-rich and the rims Ta-rich [3], but it remains to be verified whether an opposite zoning pattern occurs in P-rich deposits such as Argemela or Golpejas.

#### 6.4.2. Nb-Ta-Poor Granites

The best studied Nb-Ta-poor granite is from Logrosán [54,77]. The mineralization consists of stockworks and disseminations in altered rocks (endogreisen and host rock) enriched in Sn and slightly enriched in Nb-Ta, the so-called oxide–silicate stage. At this stage, first Nb-Ta oxides and then cassiterite precipitated. This stage is related to the mixing of magmatic and metamorphic fluids, which increased the  $fO_2$  and triggered the precipitation of cassiterite. It is worth mentioning that the granite melt must have contained a large amount of B, as abundant small q-tourmaline veins without preferred strain and tourmaline were found to occur in the granite and in the host rock, which are typical of B-rich melts and boron-dominated greisen deposits. This type of deposit has high volatile content, which induces cupola fracturing, fluid exsolution, and ore mobilization.

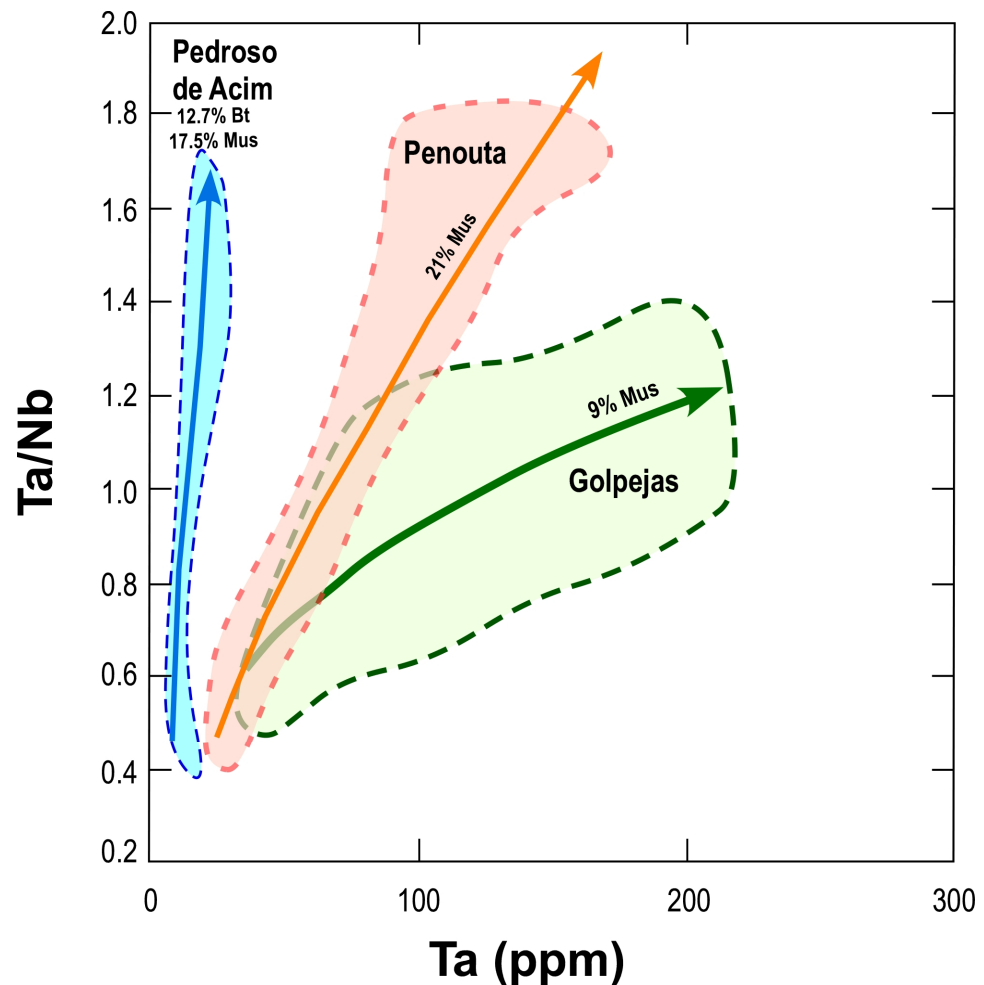


**Figure 15.** Effect of mica fractionation in Ta and Nb for three Iberian RMGs (Pedroso de Acim, Penouta, and Golpejas). Note how the different proportion and type of fractionated mica in each deposit conditions the inclination of the evolutionary trends. The modeling was done in two steps: first the proportion of fractionated phases was determined by mass balance using major elements and the OPTIMASBA code of [93] (see Table S4 for results), and then the evolution of the melt was determined by Rayleigh fractionation using the FC-AFC-FCA code [94] and the proportions of fractionated phases estimated by mass balance in Table S4. Sample 6053 at Penouta, FAD007 at Golpejas, and PA-1 at Pedroso de Acim (Table S4) were considered to be the least evolved from each deposit and were assumed to be the parental melt for both mass balance and Rayleigh modeling. The partition coefficients of Nb and Ta in muscovite, biotite, quartz, and alkali feldspars are taken from [160] and for garnet from the compilations of [139] and references therein. Penouta data (orange field) are from [2], Golpejas data (green field) are from [69,70], and Pedroso de Acim data (blue field) are from [74,83]. Only mica cumulate mode is shown in the figure.

## 7. Conclusions

The main features of this work are summarized as follows:

- (1) The Iberian rare metal granites can be divided into Nb-Ta-rich and Nb-Ta-poor granites in view of their contrasting intensive variables and geochemistry.
- (2) The parental magmas of the Iberian RMGs can be very diverse, mainly two-mica granites and granites with cordierite, although granodiorites could be the parental magmas of the P-poor RMGs.
- (3) Nb-Ta-rich granites are richer in Na than Nb-Ta-poor granites, which could be due to their higher content of fluxing elements such as F. In lens like bodies of 250 m thickness, such as Penouta, Na enrichment occurs from bottom to top, thereby suggesting

that fluoride has also increased towards the top. In thinner granite bodies, such as Golpejas, silica-rich cores and Na-rich margins could be the result of strong undercooling at the margins, thus triggering disequilibrium crystallization processes, as in some pegmatites.

- (4) In RMGs, fractional crystallization process explains the geochemical evolution from the less evolved facies, generally in the deeper zones, to the more evolved facies in the shallower levels. The evolution of some ore elements, such as Nb and Ta, from low- to high-evolved facies can also be explained in terms of this process, with a relevant role for micas fractionation. However, in the granites with the highest grades (Golpejas), the evolutionary trends with Nb and Ta showed some scatter by the effect of fluids.
- (5) Iberian RMGs, especially Nb-Ta-rich ones, with their low emplacement pressures, high water content, high proportion of anhydrous minerals, and sometimes with their reduced thickness, which favors undercooling processes, are very likely to undergo saturation and exsolution of fluids.
- (6) Fluid phase separation is very important for the development of mineralization in RMGs, as the fluid phase could transport halogens and metals (Li, F, Cl, W, Sn, Be, and Ta) as complexes that could precipitate to form high grade deposits at the apical zone (Penouta and Golpejas) and also in the core (Penouta). It is very likely that some RMGs have experienced early separation of the volatile phase, which would also increase the metals in the fluid relative to a late saturation scenario.
- (7) The separation of the fluid phase in RMGs is associated with the formation of snowball quartz, greisen, the fractionation of geochemical twins (Zr-Hf, Y-Ho, and Nb-Ta), and the occurrence of pegmatites interbedded with aplites in the apical part of granites. These features are especially evident in the Nb-Ta-rich RMGs.
- (8) The P content of feldspars is key to inferring gas-driven filter pressing processes (e.g., Golpejas). This process triggers the mobilization of near solidus water- and F-rich melts, and presumably metal-rich melts, to shallower levels. This mechanism could also explain the occurrence of Na-rich facies in the shallowest zones, where fluoride would accumulate.

**Supplementary Materials:** The following supporting information can be downloaded at: <https://www.mdpi.com/article/10.3390/min14030249/s1>, Table S1: Mineral chemistry of silicates and CGM. Table S2: Whole rock data of all RMG granites. Table S3: Whole rock data used in fractional crystallization modeling from granodiorite to Penouta granite. Table S4: Major element-based least squares modeling for Nb-Ta-rich and Nb-Ta-poor Iberian RMGs. Reference [161] are cited in the supplementary materials.

**Author Contributions:** Conceptualization, F.J.L.-M., A.D.-M. and S.M.T.-S.; methodology, F.J.L.-M. and A.D.-M.; software, F.J.L.-M. and A.D.-M.; validation, F.J.L.-M., A.D.-M. and S.M.T.-S.; investigation, F.J.L.-M.; writing—original draft preparation, F.J.L.-M., A.D.-M., S.M.T.-S. and T.L.-G.; writing—review and editing, T.L.-G. and T.S.-G.; visualization, F.J.L.-M.; project administration, A.D.-M. and S.M.T.-S.; funding acquisition, A.D.-M., S.M.T.-S., and T.S.-G. All authors have read and agreed to the published version of the manuscript.

**Funding:** This research was funded by the European Union Next Generation: Plan de Recuperación, Transformación y Resiliencia, Project C17.i7.CSIC-MET 2021-00-000: Critical Strategic Metals for the Energy Transition (MINECRITICAL). This research has also benefited from the project Forecasting and Assessing Europe's Strategic Raw Materials Needs, FRAME (GeoERA project, grant agreement N° 731166) and the project MINCE: Study of critical and strategic raw materials for the ecological transition and the supply of the main industrial value chains in Spain, from the Subdirección General de Minas (Ministerio para la Transición Ecológica y el Reto Demográfico).

**Data Availability Statement:** Data are contained within the article and Supplementary Materials.

**Acknowledgments:** The authors are grateful to the staff of the IGME-CSIC Lithoteque in Peñarroya for providing much of the information used in this publication. We gratefully appreciate the careful and detailed reviews of three anonymous reviewers.

**Conflicts of Interest:** The authors declare no conflicts of interest.

## References

1. López-Moro, F.J.; Díez-Montes, A.; Llorens-González, T.; Sánchez-García, T.; Timón-Sánchez, S.M. Is the kaolinization process the key to explaining the enrichment of critical metals in the apical zones of rare-metal granites? In Proceedings of the Goldschmidt 2023, Lyon, France, 10 July 2023.
2. López-Moro, F.J.; García Polonio, F.; Llorens González, T.; Sanz Contreras, J.L.; Fernández Fernández, A.; Moro Benito, M.C. Ta and Sn concentration by muscovite fractionation and degassing in a lens-like granite body: The case study of the Penouta rare-metal albite granite (NW Spain). *Ore Geol. Rev.* **2017**, *82*, 10–30. [[CrossRef](#)]
3. Llorens, T.; García Polonio, F.; López Moro, F.J.; Fernández, A.; Sanz, J.L.; Moro, M.C. Tin-tantalum-niobium mineralization in the Penouta deposit (NW Spain): Textural features and mineral chemistry to unravel the genesis and evolution of cassiterite and columbite group minerals in a peraluminous system. *Ore Geol. Rev.* **2017**, *81*, 79–95. [[CrossRef](#)]
4. Alfonso, P.; Hamid, S.A.; García-Valles, M.; Llorens, T.; López-Moro, F.J.; Tomasa, O.; Calvo, D.; Guasch, E.; Anticoi, H.; Oliva, J.; et al. Textural and mineral-chemistry constraints regarding the columbite-group minerals in the Penouta deposit: Evidences of magmatic and fluid-related processes. *Min. Mag.* **2018**, *82*, S199–S222. [[CrossRef](#)]
5. Michaud, J.A.S.; Pichavant, M. Magmatic fractionation and the magmatic-hydrothermal transition in rare metal granites: Evidence from Argemela (Central Portugal). *Geochim. Cosmochim. Acta* **2020**, *289*, 130–157. [[CrossRef](#)]
6. Wolf, M.; Romer, R.L.; Franz, L.; López-Moro, F.J. Tin in granitic melts: The role of melting temperature and protolith composition. *Lithos* **2018**, *310–311*, 20–30. [[CrossRef](#)]
7. Thomas, R.; Davidson, P.; Beurlen, H. Tantalite-(Mn) from the Borborema Pegmatite Province, northeastern Brazil: Conditions of formation and melt and fluid-inclusion constraints on experimental studies. *Miner. Depos.* **2011**, *46*, 749–759. [[CrossRef](#)]
8. London, D. Granitic pegmatites: An assessment of current concepts and directions for the future. *Lithos* **2005**, *80*, 281–303. [[CrossRef](#)]
9. London, D. A petrologic assessment of internal zonation in granitic pegmatites. *Lithos* **2014**, *184–187*, 74–104. [[CrossRef](#)]
10. London, D. Internal differentiation of rare-element pegmatites: Effects of boron, phosphorus, and fluorine. *Geochim. Cosmochim. Acta* **1987**, *51*, 403–420. [[CrossRef](#)]
11. London, D.; Hervig, R.L.; Morgan, G.B. Melt-vapor solubilities and element partitioning in peraluminous granite-pegmatite systems: Experimental results with Macusani glass at 200 MPa. *Contrib. Mineral. Petrol.* **1988**, *99*, 360–373. [[CrossRef](#)]
12. Chevychelov, V.Y.; Zaraisky, G.; Borisovsky, S.; Borkov, D. Partitioning of Ta and Nb between magmatic melt and aqueous (K,Na,H) F-containing fluid: Effects of temperature and chemical composition of the melt. EMPG-XSymposium Abstracts. *Lithos* **2004**, *73*, S17.
13. Raimbault, L.; Cuney, M.; Azencott, C.; Duthou, J.L.; Joron, J.-L. Multistage magmatic genesis of a Ta-Sn-Li mineralized granite at Beauvoir, French Massif Central: A geochemical study. *Econ. Geol.* **1995**, *90*, 548–576. [[CrossRef](#)]
14. Thomas, R.; Davidson, P. Revisiting complete miscibility between silicate melts and hydrous fluids, and the extreme enrichment of some elements in the supercritical state—Consequences for the formation of pegmatites and ore deposits. *Ore Geol. Rev.* **2016**, *72*, 1088–1101. [[CrossRef](#)]
15. Charoy, B.; Noronha, F. Multistage growth of a rare- element, volatile-rich microgranite at Argemela (Portugal). *J. Petrol.* **1996**, *37*, 73–94. [[CrossRef](#)]
16. Badanina, E.V.; Veksler, I.V.; Thomas, R.; Syritso, L.F.; Trumbull, R.B. Magmatic evolution of Li-F, rare metal granites: A case study of melt inclusions in the Khangilay complex, Eastern Transbaikalia (Russia). *Chem. Geol.* **2004**, *210*, 113–133. [[CrossRef](#)]
17. Martínez Catalán, J.R.; Schulmann, K.; Ghienne, J.F. The Mid-Variscan Allochthon: Keys from correlation, partial retrodeformation and plate-tectonic reconstruction to unlock the geometry of a non-cylindrical belt. *Earth Sci. Rev.* **2021**, *220*, 103700. [[CrossRef](#)]
18. Matte, P. The Variscan collage and orogeny (480-290 Ma) and the tectonic definition of the Armorica microplate: A review. *Terra Nova* **2001**, *13*, 122–128. [[CrossRef](#)]
19. Sánchez Martínez, S.; Arenas, R.; García, F.D.; Martínez-Catalán, J.R.; Gómez-Barreiro, J.; Pearce, J.A. Careón ophiolite, NW Spain: Suprasubduction zone setting for the youngest Rheic Ocean floor. *Geology* **2007**, *35*, 53–56. [[CrossRef](#)]
20. Escuder Viruete, J.; Arenas, R.; Martínez-Catalán, J.R. Tectonothermal evolution associated with Variscan crustal extension in the Tormes Gneiss Dome (NW Salamanca, Iberian Massif, Spain). *Tectonophysics* **1994**, *238*, 117–138. [[CrossRef](#)]
21. Gapais, D.; Lagarde, J.L.; Le Corre, C.; Audren, C.; Jégouzo, P.; Casas Saintz, A.; Van Den Driessche, J. La zone de cisaillement de Quiberon: Témoin d’extension de la chaîne varisque en Bretagne méridionale au Carbonifère. *CR Acad. Sci. II A* **1993**, *316*, 1123–1129.
22. Gapais, D.; Brun, J.P.; Gumiaux, C.; Cagnard, F.; Ruffet, G.; Le Carlier De Veslud, C. Extensional tectonics in the Hercynian Armorican belt (France). An overview. *BSGF* **2015**, *186*, 117–129. [[CrossRef](#)]
23. Matte, P. La chaîne varisque parmi les chaînes paleozoïques peri atlantiques, modele d’évolution et position des grands blocs continentaux au Permo-Carbonifère. *BSGF* **1986**, *II*, 9–24. [[CrossRef](#)]
24. Faure, M. Late orogenic carboniferous extensions in the Variscan French Massif Central. *Tectonics* **1995**, *14*, 132–153. [[CrossRef](#)]
25. Capdevila, R. Le métamorphisme Régional Progressif et les Granites dans le Segment Hercynien de Galice Nord Oriental (NW de l’Espagne). Ph.D. Thesis, University Montpellier, Montpellier, France, 1969.

26. Capdevila, R.; Floor, P. Les différents types de granites hercyniens et leur distribution dans le Nord-Ouest de l'Espagne. *Boletín Geológico Y Min.* **1970**, *81*, 215–225.
27. Capdevila, R.; Corretge, G.; Floor, P. Les granitoides varisques de la Meseta Iberique. *Bull. Soc. Géol. Fr.* **1973**, *15*, 209–228. [[CrossRef](#)]
28. López Plaza, M.; Martínez Catalán, J.R. Síntesis estructural de los granitoides del Macizo Hespérico. In *Geología de los Granitoides y Rocas Asociadas del Macizo Hespérico*; Bea, F., Carnicero, A., Gonzalo, J.C., López Plaza, M., Rodríguez Alonso, M.D., Eds.; Editorial Rueda: Madrid, Spain, 1987; pp. 195–210.
29. Bellido Mulas, F.; González Lodeiro, F.; Klein, E.; Martínez Catalán, J.R.; Pablo Maciá, J.G. Las rocas graníticas hercínicas del norte de Galicia y occidente de Asturias. *Colección Mem. Inst. Geológico Y Min. España* **1987**, *101*, 1–157.
30. Villaseca, C. On the origin of granite types in the Central Iberian Zone: Contribution from integrated U-Pb and Hf isotope studies of zircon. In Proceedings of the VIII Congreso Ibérico de Geoquímica, Castelo Branco, Portugal, 24–28 September 2011; pp. 271–276.
31. Roda-Robles, E.; Villaseca, C.; Pesquera, A.; Gil-Crespo, P.P.; Vieira, R.; Lima, A.; Garate-Olave, I. Petrogenetic relationships between Variscan granitoids and Li-(F-P)-rich aplite-pegmatites in the Central Iberian Zone: Geological and geochemical constraints and implications for other regions from the European Variscides. *Ore Geol. Revs.* **2018**, *95*, 408–430. [[CrossRef](#)]
32. Villaseca, C.; Bellido, F.; Pérez-Soba, C.; Billström, K. Multiple crustal sources for post-tectonic I-type granites in the Hercynian Iberian Belt. *Mineral. Petrol.* **2009**, *96*, 197–211. [[CrossRef](#)]
33. Dallmeyer, R.D.; Gil Ibarguchi, J.I. Age of amphibolitic metamorphism in the ophiolitic unit of the Morais allochthon (Portugal): Implications for early Hercynian orogenesis in the Iberian Massif. *J. Geol. Soc.* **1990**, *147*, 873–878. [[CrossRef](#)]
34. Dallmeyer, R.D.; Martínez Catalán, J.R.; Arenas, R.; Gil Ibarguchi, J.I.; Gutiérrez Alonso, G.; Farias, P.; Aller, J.; Bastida, F. Diachronous Variscan tectonothermal activity in the NW Iberian Massif: Evidence from  $^{40}\text{Ar}/^{39}\text{Ar}$  dating of regional fabrics. *Tectonophysics* **1997**, *277*, 307–337. [[CrossRef](#)]
35. Rodríguez, J.; Cosca, M.A.; Gil Ibarguchi, J.I.; Dallmeyer, R.D. Strain partitioning and preservation of  $^{40}\text{Ar}/^{39}\text{Ar}$  ages during Variscan exhumation of a subducted crust (Malpica-Tui complex, NW Spain). *Lithos* **2003**, *70*, 111–139. [[CrossRef](#)]
36. Pérez-Estaún, A.; Bea, F. Macizo Ibérico. In *Geología de España*; Vera, J.A., Ed.; Sociedad Geológica de España-Instituto Geológico y Minero de España (SGE-IGME): Madrid, Spain, 2004; pp. 19–230.
37. Valle-Aguado, B.; Azevedo, M.R.; Schaltegger, U.; Martínez Catalán, J.R.; Nolan, J. U-Pb zircon and monazite geochronology of Variscan magmatism related to syn-convergence extension in Central Northern Portugal. *Lithos* **2005**, *82*, 169–184. [[CrossRef](#)]
38. Dias, G.; Leterrier, J.; Mendes, A.; Simões, P.P.; Bertrand, J.M. U-Pb zircon and monazite geochronology of syn- to post-tectonic Hercynian granitoids from the central Iberian Zone (northern Portugal). *Lithos* **1998**, *45*, 349–369. [[CrossRef](#)]
39. Fernández-Suárez, J.; Dunning, G.R.; Jenner, G.A.; Gutiérrez-Alonso, G. Variscan collisional magmatism and deformation in NW Iberia: Constraints from U-Pb geochronology of granitoids. *J. Geol. Soc.* **2000**, *157*, 565–576. [[CrossRef](#)]
40. Serrano Pinto, M.; Casquet, C.; Ibarrola, E.; Corretgé, L.G.; Portugal Ferreira, M. Síntese geocronológica dos granitoides do Maciço Hespérico. In *Geología de los Granitoides y Rocas Asociadas del Macizo Hespérico*; Bea, F., Carnicero, A., Gonzalo, J.C., López Plaza, M., Rodríguez Alonso, M.D., Eds.; Rueda: Madrid, Spain, 1987; pp. 69–86.
41. Gallastegui, G. *Petrología del Macizo Granodiorítico de Bayo-Vigo (Provincia de Pontevedra, España)*; Serie Nova Terra; Laboratorio Xeolóxico de Laxe, Instituto Universitario de Xeoloxía: A Coruña, Spain, 2005; pp. 1–414.
42. López-Moro, F.J.; López-Plaza, M.; Gutiérrez-Alonso, G.; Fernández-Suárez, J.; López-Carmona, A.; Hofmann, M.; Romer, R.L. Crustal melting and recycling: Geochronology and sources of Variscan syn-kinematic anatectic granitoids of the Tormes Dome (Central Iberian Zone). A U-Pb LA-ICP-MS study. *Int. J. Earth Sci.* **2017**, *107*, 985–1004. [[CrossRef](#)]
43. Gutiérrez-Alonso, G.; Fernández-Suárez, J.; López-Carmona, A.; Gärtner, A. Exhuming a cold case: The early granodiorites of the northwest Iberian Variscan belt—A Visean magmatic flare-up? *Lithosphere* **2018**, *10*, 194–216. [[CrossRef](#)]
44. Valverde-Vaquero, P.; Díez Balda, M.A.; Díez-Montes, A.; Dörr, W.; Escuder Viruete, J.; González Clavijo, E.; Maluski, H.; Rodríguez-Fernández, L.R.; Rubio, F.; Villar, P. The “hot orogen”: Two separate variscan low-pressure metamorphic events in the Central Iberian Zone. Mechanics of Variscan Orogeny: A Modern View on Orogenic Research. In *Géologie de la France*; Faure, M., Lardeaux, J.-M., Ledru, P., Peschler, A., Schulmann, K., Eds.; Société Géologique de France and Bureau de Recherches Géologiques et Minière: Orleans, France, 2007; Volume 2, p. 168.
45. Díez Montes, A. *La Geología del Dominio “Ollo de Sapo” en las Comarcas de Sanabria y Terra do Bolo*; Serie Nova Terra; Laboratorio Xeolóxico de Laxe, Instituto Universitario de Xeoloxía: A Coruña, Spain, 2007; Volume 34, pp. 1–494.
46. Gutiérrez-Alonso, G.; Collins, A.S.; Fernández-Suárez, J.; Pastor-Galán, D.; González-Clavijo, E.; Jourdan, F.; Weil, A.B.; Johnston, S.T. Dating of lithospheric buckling:  $^{40}\text{Ar}/^{39}\text{Ar}$  ages of syn-orocline strike-slip shear zones in northwestern Iberia. *Tectonophysics* **2015**, *643*, 44–54. [[CrossRef](#)]
47. Bea, F.; Montero, P.G.; González-Lodeiro, F.; Talavera, C.; Molina, J.F.; Scarrow, J.H.; Whitehouse, M.J.; Zinger, T. Zircon thermometry and U-Pb ion-microprobe dating of the gabbros and associated migmatites of the Variscan Toledo Anatectic Complex, Central Iberia. *J. Geol. Soc.* **2006**, *163*, 847–855. [[CrossRef](#)]
48. Orejana, D.; Villaseca, C.; Pérez-Soba, C.; López-García, J.A.; Billström, K. The Variscan gabbros from the Spanish Central System: A case for crustal recycling in the sub-continental lithospheric mantle? *Lithos* **2009**, *110*, 262–276. [[CrossRef](#)]

49. Gutiérrez-Alonso, G.; Fernández-Suárez, J.; Jeffries, T.E.; Johnston, S.T.; Pastor-Galán, D.; Murphy, J.B.; Franco, M.P.; Gonzalo, J.C. Diachronous post-orogenic magmatism within a developing orocline in Iberia, European Variscides. *Tectonics* **2011**, *30*, TC5008. [[CrossRef](#)]
50. González Menéndez, L.; Gallastegui, G.; Cuesta, A.; Montero, P.; Rubio-Ordóñez, A.; Molina, J.F.; Bea, F. Petrology and geochronology of the Porriño late-Variscan pluton from NW Iberia. A model for post-tectonic plutons in collisional settings. *Geol. Acta* **2017**, *15*, 283–304.
51. Orejana, D.; Villaseca, C.; Kristoffersen, M. Geochemistry and geochronology of mafic rocks from the Spanish Central System: Constraints on the mantle evolution beneath central Spain. *Geosci. Front.* **2020**, *11*, 1651–1667. [[CrossRef](#)]
52. Melleton, J.; Gloaguen, E.; Frei, D.; Lima, A.; Vieira, R.; Martins, T. Polyphased rare-element magmatism during late orogenic evolution: Geochronological constraints from NW Variscan Iberia. *Bull. Soc. Geol. Fr. Earth Sci. Bull.* **2022**, *193*, 7. [[CrossRef](#)]
53. Orejana, D.; Merino, E.; Villaseca, C.; Pérez-Soba, C.; Cuesta, A. Electron microprobe monazite geochronology of granitic intrusions from the Montes de Toledo batholith (central Spain). *Geol. J.* **2012**, *47*, 41–58. [[CrossRef](#)]
54. Chicharro, E. Petrologic-metallogenic characterization of a specialized granite: The Logrosán stock (Cáceres). Ph.D. Thesis, Universidad Complutense de Madrid, Madrid, Spain, 2016.
55. Chauris, L. Beryl leucogranites from southern Brittany. In Proceedings of the 113th National Congress of Learned Societies, Earth Sciences, Strasbourg, France, 1988; pp. 37–49.
56. Raimbault, L. Composition of complex lepidolite-type granitic pegmatites and of constituent columbite-tantalite, Chedeville, Massif Central, France. *Can. Mineral.* **1998**, *36*, 563–583.
57. Raimbault, L.; Charoy, B.; Cuney, M.; Pollard, P.J. Comparative geochemistry of Ta-bearing granites. In *Source, Transport and Deposition of Metals*; Pagel, M., Leroy, J.L., Eds.; Society for Geology Applied to Mineral Deposits: Nancy, France, 1991; pp. 793–796.
58. Aubert, G. *Les Coupoles Granitiques de Montebras et d'Échassières (Massif Central français) et la Genèse de Leurs Minéralisations en étain, Lithium, Tungstène et Beryllium*; BRGM: Orléans, France, 1969.
59. Breiter, K.; Durisová, J.; Korbelová, Z.; Lima, A.; Vasinová Galiová, M.; Hložková, M.; Dosebaba, M. Rock textures and mineral zoning—A clue to understanding rare-metal granite evolution: Argemela stock, Central-Eastern Portugal. *Lithos* **2022**, *410–411*, 106562. [[CrossRef](#)]
60. Breiter, K.; Müller, A.; Leichmann, J.; Gabašová, A. Textural and chemical evolution of a fractionated granitic system: The Podlesí stock, Czech Republic. *Lithos* **2005**, *80*, 323–345. [[CrossRef](#)]
61. Breiter, K.; Durisová, J.; Hrstka, T.; Korbelová, Z.; Hložková Vanková, M.; Vasinová Galiová, M.; Kanický, V.; Rambousek, P.; Knésl, I.; Dobes, P.; et al. Assessment of magmatic vs. metasomatic processes in rare-metal granites: A case study of the Cínovec/Zinnwald Sn–W–Li deposit, Central Europe. *Lithos* **2017**, *292–293*, 198–217. [[CrossRef](#)]
62. Manning, D.A.C.; Hill, P.I. The petrogenetic and metallogenic significance of topaz granite from the Southwest England orefield. *Geol. Soc. Am. Spec.* **1990**, *246*, 51–69.
63. Müller, A.; Seltsmann, R.; Halls, C.; Siebel, W.; Dulski, P.; Jeffries, T.; Spratt, J.; Kronz, A. The magmatic evolution of the Land's End pluton, Cornwall, and associated pre-enrichment of metals. *Ore Geol. Rev.* **2006**, *28*, 329–367. [[CrossRef](#)]
64. Michaud, J.A. Rare Metal Granites Origin, Emplacement and Mechanisms of the Magmatic-Hydrothermal Transition—Insights from the Argemela Rare Metal Granite (Portugal) and an Experimental Study. Ph.D. Thesis, University D'Orléans, Orléans, France, 2019.
65. Gonzalo Corral, F.J.; Gracia Plaza, A.S. Yacimientos de estaño del Oeste de España. *Cad. Do Lab. Xeolóxico De Laxe* **1985**, *9*, 265–303.
66. Franke, W. Variscan plate tectonics in Central Europe—current ideas and open questions. *Tectonophysics* **1989**, *169*, 221–228. [[CrossRef](#)]
67. Minera del Duero. *Mining Work Mina Bellita and Tita (Golpejas): Final Report*, 1985. (In Spanish)
68. ADARO. Penouta deposit mining research. *Geological Characteristics and Reserves*, Final Report. 1985; Volume I, 1–123. (In Spanish)
69. Reginiussen, H.; Jonsson, E.; Hamisi, J.; Timón-Sánchez, S.M.; Díez-Montes, A.; Teran, K.; Salgueiro, R.; Oliveira, D.; Melnik, I. Providing data and intelligence on Nb-Ta mineralizations in Europe to the GeoERA information platform. In *FRAME WP6*; Appendix 1. Analytical data Spanish deposits, D6.4. 26p; 2021; 220p.
70. Solid Mines España. *Alberta 5 Golpejas-Salamanca Tin-Tantalum Project*, Internal report. 2005.
71. Armstrong, E.; Murillo, A.; Pages, J.L. Investigación minera por estaño en la reserva nº 146 “Villardecervos” (Orense). *Cad. Do Lab. Xeolóxico De Laxe* **1983**, *6*, 459–467.
72. ITGE. Estimation of the mining potential in the area of Villardevós (ORENSE). Annex 1, Methodology and content sheets. *Final Report*, 1976. (In Spanish)
73. López-Plaza, M.; Rodríguez Alonso, M.D.; Martín Herrero, D.; Albert Colomert, V. *Mapa Geológico y Memoria de la Hoja nº 525 (Ciudad Rodrigo)*; 2ª serie del Mapa Geológico Nacional a escala 1:50.000 (MAGNA); Servicio de Publicaciones IGME: Madrid, Spain, 1990; pp. 1–96.
74. Gallego Garrido, M. Las Mineralizaciones de Litio Asociadas a Magmatismo Ácido en Extremadura y su Encuadre en la Zona Centro-Ibérica. Ph.D. Thesis, Universidad Complutense de Madrid, Madrid, Spain, 1992.
75. Garate-Olave, I.; Roda-Robles, E.; Gil-Crespo, P.P.; Pesquera, A.; Errandonea-Martin, J. The Tres Arroyos granitic aplite-pegmatite field (Central Iberian Zone, Spain): Petrogenetic constraints from evolution of Nb-Ta-Sn oxides, whole-rock geochemistry and U-Pb geochronology. *Minerals* **2020**, *10*, 1008. [[CrossRef](#)]

76. IGME. Project: Expansion of the intermediate phase of Sn-W mining research in several areas of Extremadura. In *Final Report*; El Tráquilón Area: Cáceres, Spain, 1980. (In Spanish)
77. Chicharro, E.; Boiron, M.C.; López García, J.A.; Barfold, D.N.; Villaseca, C. Origin, ore forming fluid evolution and timing of the Logrosán Sn–(W) ore deposits (Central Iberian Zone, Spain). *Ore Geol. Rev.* **2016**, *72*, 896–913. [[CrossRef](#)]
78. ITGE. Basic Study of Tin Deposits. Type-Laza. Memory-annexes and maps. In *Final Report*; 1976; pp. 1–149. (In Spanish)
79. Canosa, F.; Martín-Izard, A.; Fuertes-Fuente, M. Evolved granitic systems as a source of rare-element deposits: The Ponte Segade case (Galicia, NW Spain). *Lithos* **2012**, *153*, 165–176. [[CrossRef](#)]
80. Gloaguen, E. Apports D’une Étude Intégrée su les Relations Entre Granites et Minéralisations Filoniennes (Au et Sn-W) en contexte Tardi Orogénique (Chaîne Hercynienne, Galice Centrale, Espagne). Ph.D. Thesis, University of D’Orleans, Orléans, France, 2006.
81. González Aguado, M.T. Mineralizaciones de Sn-Nb-Ta Asociadas a Cúpulas Graníticas de Extremadura. Ph.D. Thesis, Escuela Técnica Superior de Ingenieros de Minas, Madrid, Spain, 1985.
82. Merino, E.; Villaseca, C.; Orejana, D.; Jeffries, T. Gahnite, chrysoberyl and beryl co-occurrence as accessory minerals in a highly evolved peraluminous pluton: The Belvís de Monroy leucogranite (Cáceres, Spain). *Lithos* **2013**, *179*, 137–156. [[CrossRef](#)]
83. ADARO. ADARO. Research Project for tin and wolfram on the permit “MARIVI” Pedroso de Acim (Cáceres). In *Final Report*; 1984; Volume 1, pp. 1–215. (In Spanish)
84. Ramírez, J.A.; Grundvig, S. Causes of geochemical diversity in peraluminous granitic plutons: The Jálama pluton, Central-Iberian Zone (Spain and Portugal). *Lithos* **2000**, *50*, 171–190. [[CrossRef](#)]
85. Díez-Montes, A.; Martínez Catalán, J.R.; Bellido Mulas, F. Role of the Ollo de Sapo massive felsic volcanism of NW Iberia in the Early Ordovician dynamics of northern Gondwana. *Gondwana Res.* **2010**, *17*, 363–376. [[CrossRef](#)]
86. Arribas, A.; Gonzalo Corral, F.J.; Iglesias, M. Génesis de una mineralización asociada a una cúpula granítica: El yacimiento de estaño de Golpejas, (Salamanca). *Cad. Do Lab. Xeolóxico De Laxe* **1982**, *3*, 563–592.
87. Watson, E.B.; Harrison, T.M. Zircon saturation revisited: Temperature and compositional effects in a variety of crustal magma types. *Earth Planet. Sci. Lett.* **1983**, *64*, 295–304. [[CrossRef](#)]
88. Montel, J.M. A model for monazite/melt equilibrium and application to the generation of granitic magmas. *Chem. Geol.* **1993**, *110*, 127–146. [[CrossRef](#)]
89. Pichavant, M.; Montel, J.M.; Richard, L.R. Apatite solubility in peraluminous liquids: Experimental data and an extension of the Harrison-Watson model. *Geochim. Cosmochim. Acta* **1992**, *56*, 3855–3861. [[CrossRef](#)]
90. Massonne, H.J.; Schreyer, W. Phengite geobarometry based on the limiting assemblage with k-feldspar, phlogopite, and quartz. *Contrib. Mineral. Petrol.* **1987**, *96*, 212–224. [[CrossRef](#)]
91. Moore, G.; Vennemann, T.; Carmichael, I.S.E. An empirical model for the solubility of H<sub>2</sub>O in magmas to 3 kilobars. *Am. Mineral.* **1998**, *83*, 36–42. [[CrossRef](#)]
92. Gualda, G.A.R.; Ghiorsio, M.S.; Lemons, R.V.; Carley, T. Rhyolite-MELTS: A Modified Calibration of MELTS Optimized for Silica-rich, Fluid-bearing Magmatic Systems. *J. Petrol.* **2012**, *53*, 875–890. [[CrossRef](#)]
93. Cabero, M.T.; Mecoleta, S.; López-Moro, F.J. OPTIMASBA: A Microsoft Excel workbook to optimise the mass-balance modelling applied to magmatic differentiation processes and subsolidus overprints. *Comput. Geosci.* **2012**, *42*, 206–211. [[CrossRef](#)]
94. Ersoy, E.Y.; Helvacı, C. FC–AFC–FCA and mixing modeler: A Microsoft®Excel® spreadsheet program for modeling geochemical differentiation of magma by crystal fractionation, crustal assimilation and mixing. *Comput. Geosci.* **2010**, *36*, 383–390. [[CrossRef](#)]
95. London, D. Phosphorus in S-type magmas: The P<sub>2</sub>O<sub>5</sub> content of feldspars from peraluminous granites, pegmatites, and rhyolites. *Am. Mineral.* **1992**, *77*, 126–145.
96. London, D.; Morgan VI, G.B.; Babb, H.A.; Loomis, J.L. Behavior and effects of phosphorus in the system Na<sub>2</sub>O–K<sub>2</sub>O–Al<sub>2</sub>O<sub>3</sub>–SiO<sub>2</sub>–P<sub>2</sub>O<sub>5</sub>–H<sub>2</sub>O at 200 MPa (H<sub>2</sub>O). *Contrib. Mineral. Petrol.* **1993**, *113*, 450–465. [[CrossRef](#)]
97. Tischendorf, G.; Gottesmann, B.; Förster, H.-J.; Trumbull, R.B. On Li-bearing micas: Estimating Li from electron microprobe analyses and an improved diagram for graphical representation. *Min. Mag.* **1997**, *61*, 809–834. [[CrossRef](#)]
98. Van Lichtervelde, M.; Holtz, F.; Melcher, F. The effect of disequilibrium crystallization on Nb-Ta fractionation in pegmatites: Constraints from crystallization experiments of tantalite-tapiolite. *Am. Min.* **2018**, *103*, 1401–1416. [[CrossRef](#)]
99. Frost, B.R.; Frost, C.D. A geochemical classification for feldspathic igneous rocks. *J. Petrol.* **2008**, *49*, 1955–1969. [[CrossRef](#)]
100. Linnen, R.L.; Cuney, M. Granite-related rare-element deposits and experimental constraints on Ta-Nb-W-Sn-Zr-Hf mineralization. In *Rare-Element Geochemistry and Mineral Deposits*; GAC Short Course Notes; Linnen, R.L., Samson, I.M., Eds.; Geological Association of Canada: St. John’s, NL, Canada, 2005; Volume 17, pp. 45–67.
101. Debon, F.; Le Fort, P. A chemical mineralogical classification of common plutonic rocks and association. *Earth Sci.* **1983**, *73*, 135–149. [[CrossRef](#)]
102. Whalen, J.B.; Currie, K.L.; Chappell, B.W. A-type granites: Geochemical characteristics, discrimination and petrogenesis. *Contrib. Mineral. Petrol.* **1987**, *95*, 407–419. [[CrossRef](#)]
103. Pearce, J.A.; Harris, N.B.W.; Tindle, A.G. Trace element discrimination diagrams for the tectonic interpretation of granitic rocks. *J. Petrol.* **1984**, *25*, 956–983. [[CrossRef](#)]
104. Eby, G.N. The A-type granitoids: A review of their occurrence and chemical characteristics and speculations on their petrogenesis. *Lithos* **1990**, *26*, 115–134. [[CrossRef](#)]
105. Maniar, P.D.; Piccoli, P.M. Tectonic discrimination of granitoids. *Geol. Soc. Am. Bull.* **1989**, *101*, 635–643. [[CrossRef](#)]

106. Villaseca, C.; Barbero, L.; Herrerros, V. A re-examination of the typology of peraluminous granite types in intracontinental orogenic belts. *Trans. RSE. Earth* **1998**, *89*, 113–119. [[CrossRef](#)]
107. Ballouard, C.; Poujol, M.; Boulvais, P.; Branquet, Y.; Tartèse, R.; Vignerresse, J.L. Nb-Ta fractionation in peraluminous granites: A marker of the magmatic-hydrothermal transition. *Geology* **2016**, *44*, 231–234. [[CrossRef](#)]
108. Förster, H.-J.; Rhede, D. The Be–Ta-rich granite of Seiffen (eastern Erzgebirge, Germany): Accessory-mineral chemistry, composition, and age of a late-Variscan Li–F granite of A-type affinity. *Neues Jahrb. Für Mineral. Abh.* **2006**, *182*, 307–321.
109. Rudnick, R.L.; Fountain, D. Nature and composition of the continental crust: A lower crustal perspective. *Rev. Geophys.* **1995**, *33*, 267–309. [[CrossRef](#)]
110. Taylor, S.R.; McLennan, S.M. *The Continental Crust: Its Composition and Evolution*; Blackwell: Oxford, UK, 1985.
111. Bau, M. Controls on the fractionation of isovalent trace elements in magmatic and aqueous systems: Evidence from Y/Ho, Zr/Hf, and lanthanide tetrad effect. *Contrib. Mineral. Petrol.* **1996**, *123*, 323–333. [[CrossRef](#)]
112. Sun, S.S.; McDonough, W.F. Chemical and isotopic systematics of oceanic basalts: Implications for mantle composition and processes. In *Magmatism in Ocean Basins*; Geological Society Special, Publication; Saunders, A.D., Norrly, M.J., Eds.; Geological Society: London, UK, 1989; Volume 42, pp. 313–345.
113. Irber, W. The lanthanide tetrad effect and its correlation with K/Rb, Eu/Eu, Sr/Eu, Y/Ho and Zr/Hf of evolving peraluminous granite suits. *Geochim. Cosmochim. Acta* **1999**, *63*, 489–508. [[CrossRef](#)]
114. González Menéndez, L.; Bea, F. El batolito de Nisa-Alburquerque. In *Geología de España*; Vera, J.A., Ancochea, A., Calvo Sorando, J.P., Barnolas Cortinas, A., Bea Carredo, F., Eds.; SGE-IGME: Madrid, Spain, 2004; pp. 120–122.
115. López-Moro, F.J.; López-Plaza, M.; Romer, R.L. Generation and emplacement of shear-related highly mobile crustal melts: The synkinematic leucogranites from the Variscan Tormes Dome, Western Spain. *Int. J. Earth Sci.* **2012**, *101*, 1273–1298. [[CrossRef](#)]
116. Pichavant, M. Experimental Crystallization of the Beauvoir Granite as a Model for the Evolution of Variscan Rare Metal Magmas. *J. Petrol.* **2023**, *63*, egac120. [[CrossRef](#)]
117. Piccoli, P.; Candela, P. Apatite in igneous systems. In *Phosphates: Geochemical, Geobiological, and Materials Importance*; Kohn, M.J., Rakovan, J., Hughes, J.M., Eds.; Reviews in Mineralogy and Geochemistry; Mineralogical Society of America: Washington, DC, USA, 2002; Volume 48, pp. 255–292.
118. Mangas, J.; Arribas, A. Fluid inclusion study in different types of tin deposits associated with the Hercynian granites of western Spain. *Chem. Geol.* **1987**, *61*, 193–208. [[CrossRef](#)]
119. Candela, P.A. A Review of Shallow, Ore-related Granites: Textures, Volatiles, and Ore Metals. *J. Petrol.* **1997**, *38*, 1619–1633. [[CrossRef](#)]
120. Oppenheimer, C.; Fischer, T.P.; Scaillet, B. 4.4.- Volcanic degassing: Process and impact. In *Treatise on Geochemistry, 2nd ed*; Holland, H.D., Turekian, K.K., Eds.; Elsevier: Amsterdam, The Netherlands, 2014; Volume 4, pp. 111–179.
121. Villaseca, C.; Pérez-Soba, C.; Merino, E.; Orejana, D.; López-García, J.A.; Billström, K. Contrasting crustal sources for peraluminous granites of the segmented Montes de Toledo Batholith (Iberian Variscan Belt). *J. Geosci.* **2008**, *53*, 263–280.
122. Bickle, M.J.; Wickham, S.M.; Chapman, H.J.; Taylor, H.P., Jr. A strontium, neodymium and oxygen isotope study of hydrothermal metamorphism and crustal anatexis in the Trois Seigneurs Massif, Pyrenees, France. *Contrib. Mineral. Petrol.* **1988**, *100*, 399–417. [[CrossRef](#)]
123. Villaseca, C.; Barbero, L.; Rogers, G. Crustal origin of Hercynian peraluminous granitic batholiths of Central Spain: Petrological, geochemical and isotopic (Sr, Nd) constraints. *Lithos* **1998**, *43*, 55–79. [[CrossRef](#)]
124. Jung, S. Isotopic equilibrium/disequilibrium in granites, metasedimentary rocks and migmatites (Damara orogen, Namibia)—A consequence of polymetamorphism and melting. *Lithos* **2005**, *84*, 168–184. [[CrossRef](#)]
125. Zeng, L.; Asimow, P.D.; Saleeby, J.B. Coupling of anatectic reactions and dissolution of accessory phases and the Sr and Nd isotope systematics of anatectic melts from a metasedimentary source. *Geochim. Cosmochim. Acta* **2005**, *69*, 3671–3682. [[CrossRef](#)]
126. Vásquez, P.; Glodny, J.; Franz, G.; Romer, R.L.; Gerdes, A. Origin of fayalite granitoids: New insights from the Cobquecura Pluton, Chile, and its metapelitic xenoliths. *Lithos* **2009**, *110*, 181–198. [[CrossRef](#)]
127. Ballouard, C.; Couzinié, S.; Bouilhol, P.; Harlaux, M.; Mercadier, M.; Montel, J.M. A felsic meta-igneous source for Li-F-rich peraluminous granites: Insights from the Variscan Velay dome (French Massif Central) and implications for rare-metal magmatism. *Contrib. Mineral. Petrol.* **2023**, *178*, 1–24. [[CrossRef](#)]
128. Fu, J.; Li, G.; Wang, G.; Guo, W.; Dong, S.; Li, Y.; Zhang, H.; Liang, W.; Jiao, Y. Geochemical Evidence for Genesis of Nb-Ta-Be Rare Metal Mineralization in Highly Fractionated Leucogranites at the Lalong Dome, Tethian Himalaya, China. *Minerals* **2023**, *13*, 1456. [[CrossRef](#)]
129. Tischendorf, G.; Förster, H.-J. Acid magmatism and related metallogenesis in the Erzgebirge. *Geol. J.* **1990**, *25*, 443–454. [[CrossRef](#)]
130. Teuscher, E.O. Primäre Bildungen des granitischen Magmas und seiner Restlösungen im Massif von Eibenstock-Neudeck. *Mineral. Und Petrogr. Mitteilungen* **1936**, *47*, 211–262. [[CrossRef](#)]
131. Beus, A.A.; Zhalashkova, N.Y. Postmagmatic high temperature metasomatic processes in granitic rocks. *Int. Geol. Rev.* **1964**, *6*, 668–681. [[CrossRef](#)]
132. Kovalenko, V.I.; Kuzmin, M.I.; Antipin, V.S.; Petrov, I.I. Topaz-bearing quartz keratophyre (ongonite): A new variety of subvolcanic igneous dike rocks. *Dokl. Akad. Nauk. SSSR Earth Sci. Sect.* **1971**, *199*, 132–135.
133. London, D.; Morgan, C.B.; Hervig, R.I. Vapour-undersaturated experiments with Macusani glass+ H<sub>2</sub>O at 200 MPa, and their internal differentiation of granitic pegmatites. *Contrib. Mineral. Petrol.* **1989**, *102*, 1–17. [[CrossRef](#)]

134. Pichavant, M.; Kontak, D.J.; Herrera, J.V.; Clarke, A.H. The Miocene–Pliocene Macusani volcanics, SE Peru, II. Geochemistry and origin of a felsic peraluminous magma. *Contrib. Mineral. Petrol.* **1988**, *100*, 325–338. [[CrossRef](#)]
135. Manning, D.A.C. The effect of fluorine on liquidus phase relationships in the system Qz–Ab–Or with excess water at 1 Kb. *Contrib. Mineral. Petrol.* **1981**, *76*, 206–215. [[CrossRef](#)]
136. Thomas, R.; Webster, J.D. Strong tin enrichment in a pegmatite-forming melt. *Miner. Depos.* **2000**, *35*, 570–582. [[CrossRef](#)]
137. Romer, R.L.; Kroner, U. Sediment and weathering control on the distribution of Paleozoic magmatic tin-tungsten mineralization. *Miner. Depos.* **2015**, *50*, 327–338. [[CrossRef](#)]
138. Rollinson, H.; Pease, V. *Using Geochemical Data: To Understand Geological Processes*; Cambridge University Press: Cambridge, UK, 2021.
139. GERM Partition Coefficient (Kd) Database. Available online: <https://earthref.org/KDD-old/> (accessed on 10 February 2024).
140. Luth, W.C.; Jahns, R.H.; Tuttle, O.F. The granite system at pressures of 4 to 10 kilobars. *J. Geophys. Res.* **1964**, *69*, 759–773. [[CrossRef](#)]
141. López-Plaza, M.; López-Moro, F.J. *Eurogranites in Western Castilla y León, Spain: The Tormes Dome*; University Salamanca: Salamanca, Spain, 2008; p. 193.
142. London, D. Subsolidus isothermal fractional crystallization. *Am. Mineral.* **2014**, *99*, 543–546. [[CrossRef](#)]
143. Errandonea-Martín, J.; Gárate-Olave, I.; Roda-Robles, E.; Cardoso-Fernandes, J.; Lima, A.; Ribeiro, M.; Teodoro, A.C. Metasomatic effect of Li-bearing aplite-pegmatites on psammitic and pelitic metasediments: Geochemical constraints on critical raw material exploration at the Fregeneda–Almendra Pegmatite Field (Spain and Portugal). *Ore Geol. Rev.* **2022**, *150*, 105155. [[CrossRef](#)]
144. Candela, P.A.; Holland, H.D. A mass transfer model for copper and molybdenum in magmatic hydrothermal systems: The origin of porphyry-type ore deposits. *Econ. Geol.* **1986**, *81*, 1–19. [[CrossRef](#)]
145. Wang, D.; Liu, J.; Carranza, E.J.M.; Zhai, D.; Wang, Y.; Zhen, S.; Wang, J.; Wang, J.; Liu, Z.; Zhang, F. Formation and evolution of snowball quartz phenocrysts in the Dongping porphyritic granite, Hebei Province, China: Insights from fluid inclusions, cathodoluminescence, trace elements, and crystal size distribution study. *Lithos* **2019**, *340–341*, 239–254. [[CrossRef](#)]
146. López-Moro, F.J.; Díez-Montes, A.; Llorens-González, T.; Sánchez-García, T.; Timón-Sánchez, S.M. Intensive variables in the Golpejas rare metal granite and their implications for ore mineralization. In Proceedings of the Reunión Científica de la SEM 2023, Madrid, Spain, 16 June 2023.
147. Sisson, T.W.; Bacon, C.R. Gas-driven filter pressing in magmas. *Geology* **1999**, *27*, 613–616. [[CrossRef](#)]
148. Raimbault, L.; Burnol, L. The Richemont rhyolite dyke, Massif central, France: A subvolcanic equivalent of rare-metal granites. *Can. Mineral.* **1998**, *36*, 265–282.
149. Linnen, R.L. The solubility of Nb–Ta–Zr–Hf–W in granitic melts with Li and Li+F: Constraints for mineralization in rare-metal granites and pegmatites. *Econ. Geol.* **1998**, *93*, 1013–1025. [[CrossRef](#)]
150. Bartels, A.; Holtz, F.; Linnen, R.L. Solubility of manganotantalite and manganocolumbite in pegmatitic melts. *Am. Mineral.* **2010**, *95*, 537–544. [[CrossRef](#)]
151. Taylor, J.R.P.; Wall, V.J. The behavior of tin in granitoid magmas. *Econ. Geol.* **1992**, *87*, 403–420. [[CrossRef](#)]
152. Štemprok, M. Solubility of tin, tungsten and molybdenum oxides in felsic magmas. *Miner. Depos.* **1990**, *25*, 205–212. [[CrossRef](#)]
153. Webster, J.; Thomas, R.; Förster, H.J.; Seltmann, R.; Tappen, C. Geochemical evolution of halogen-enriched granite magmas and mineralizing fluids of the Zinnwald tin-tungsten mining district, Erzgebirge, Germany. *Miner. Depos.* **2004**, *39*, 452–472. [[CrossRef](#)]
154. Zhou, Z.; Breiter, K.; Wilde, S.A.; Gao, X.; Burnham, A.D.; Ma, X.; Zhao, J. Ta–Nb mineralization in the shallow-level highly-evolved P-poor Shihuiyao granite, Northeast China. *Lithos* **2022**, *416–417*, 106655. [[CrossRef](#)]
155. Zoheir, B.; Lehmann, B.; Emam, A.; Radwan, A.; Zhang, R.; Bain, W.M.; Steele-MacInnis, M.; Nolte, N. Extreme fractionation and magmatic–hydrothermal transition in the formation of the Abu Dabbab rare-metal granite, Eastern Desert, Egypt. *Lithos* **2020**, *352–353*, 105329. [[CrossRef](#)]
156. Zaraisky, G.P.; Korzhinskaya, V.; Kotova, N. Experimental studies of Ta<sub>2</sub>O<sub>5</sub> and columbite–tantalite solubility in fluoride solutions from 300 to 550 °C and 50 to 100MPa. *Miner. Petrol.* **2010**, *99*, 287–300. [[CrossRef](#)]
157. Tang, Y.; Zhang, H.; Rao, B. The effect of phosphorus on manganocolumbite and manganotantalite solubility in peralkaline to peraluminous granitic melts. *Am. Mineral.* **2016**, *101*, 415–422. [[CrossRef](#)]
158. Linnen, R.L. The effects of water on the solubility of accessory minerals in granitic melts. *Lithos* **2005**, *80*, 267–280. [[CrossRef](#)]
159. Linnen, R.L.; Keppler, H. Columbite solubility in granitic melts: Consequences for the enrichment and fractionation of Nb and Ta in the Earth’s crust. *Contrib. Mineral. Petrol.* **1997**, *128*, 213–227. [[CrossRef](#)]
160. Pichavant, M.; Erdmann, S.; Kontak, D.J.; Michaud, J.A.S.; Villaros, A. Trace element partitioning in strongly peraluminous rare-metal silicic magmas—Implications for fractionation processes and for the origin of the Macusani Volcanics (SE Peru). *Geochim. Cosmochim. Acta* **2024**, *365*, 229–252. [[CrossRef](#)]
161. Whitney, D.L.; Evans, B.W. Abbreviations for names of rock-forming minerals. *Am. Mineral.* **2010**, *95*, 185–187. [[CrossRef](#)]

**Disclaimer/Publisher’s Note:** The statements, opinions and data contained in all publications are solely those of the individual author(s) and contributor(s) and not of MDPI and/or the editor(s). MDPI and/or the editor(s) disclaim responsibility for any injury to people or property resulting from any ideas, methods, instructions or products referred to in the content.